INTERNATIONAL JOURNAL OF CLIMATOLOGY
Int. J. Climatol. (2015)
Published online in Wiley Online Library
(wileyonlinelibrary.com) DOI: 10.1002/joc.4302

RMetS
Royal Meteorological Society

Shamals and climate variability in the Northern Arabian/Persian Gulf from 1973 to 2012

Fahad Al Senafi and Ayal Anis*

Marine Sciences & Oceanography, Texas A&M University, Galveston, USA

ABSTRACT: This paper presents key results from analysis of surface meteorological observations collected in the Northern Arabian/Persian Gulf (N Gulf; Kuwait, Bahrain, and NE Saudi Arabia), which spans a 40-years period (1973–2012). The first part of this study analyzes climate variability in the N Gulf, and relates them to teleconnection patterns (North Atlantic Oscillation, El Nino Southern Oscillation, and Indian Ocean Dipole). Results of the analysis indicate that during the study period the climate in the region experienced a general trend of increase in temperature (0.8°C), decrease in barometric pressure (1 mbar), reduction in humidity (6%), and decrease in visibility (9%). Significant correlations were found between the three teleconnection patterns and the meteorological conditions suggesting that seasonal variabilities in air temperature, barometric pressure, and precipitation are closely related to the teleconnection patterns. The second part of this study examines the 40-year variability of Shamal events (strong NW winds that commonly generate significant dust storms). The data suggests that on average Shamal events occur at a rate of 10 events year^{-1} with 85% of the events occurring during the summer and winter. The number of these events has increased in the past 14 years of the study period. These events resulted in abrupt changes in meteorological conditions: an increase in wind speed of 2.7 m s^{-1}, a decrease in visibility of 1.7 km, and reduction in humidity of 4.3%. Seasonal variations in temperature (an increase in temperature during summer of 0.8°C, and a decrease of 1.5°C during winter) and barometric pressure (a decrease in barometric pressure during summer of 0.6 mbar and an increase of 7.8 mbar during winter) were observed during Shamal events.

KEY WORDS Shamal; Arabian Gulf; North Atlantic Oscillation; El Nino Southern Oscillation; Indian Ocean Dipole; Kuwait; climate variability; Persian Gulf

Received 17 November 2014; Revised 4 February 2015; Accepted 5 February 2015

1. Introduction

Effects of global climate change on the relative increase of surface temperatures (Jones, 2003; Attrill, 2009), droughts (van Vliet *et al.*, 2013), flooding (Mirza, 2002), and intensity of weather events such as monsoons (Naidu *et al.*, 2012) and hurricanes (Arpe and Leroy, 2009) have been increasing steadily. The rise in number of environmental catastrophes due to severe weather events in the last 50 years (Leroy, 2006) has further motivated scientists to better understand the impacts of global climate change on weather systems and phenomena (e.g. IPCC, 2014). In the Arabian/Persian Gulf (hereafter called the Gulf) (Figure 1), a unique weather phenomena occurs throughout the year and has substantial impact on the society, economy, transportation, and the natural environment; it is known as a Shamal event (details of Shamals in Section 1.2).

In this manuscript, our first aim is to describe climate variability in the N Gulf region based on three (Kuwait, Bahrain, and NE Saudi Arabia) 40-year-long datasets, covering the period from 1973 to 2012, and relate teleconnection patterns (large scale modes of climate variability) to climate variability. To the best of our knowledge, there are no published studies documenting the long-term variability of Shamal events as reported in this study. The only other long-term study of Shamals was presented by Rao *et al.* (2001). The latter study discusses the effects of Shamals on meteorological parameters (barometric pressure, wind speed, humidity, and air temperature) and quantifies the frequency of events over a decade (1990–2000) at Doha, Qatar.

The second aim is to describe the variability of Shamal events and its effect on various meteorological parameters. Shamal events have a significant impact on surface heat fluxes (shortwave, longwave, sensible, and latent), momentum fluxes, and, as a result, on vertical water column stratification, currents, and mixing intensities (Thoppil and Hogan, 2010). The importance of Shamal events in the region and the relation to climate variability has motivated the second aim of this study and an ongoing oceanographic field experiment.

To set the stage, we proceed by describing the climate characteristics in the region focusing on the seasons and the general synoptic conditions during each season (Section 1.1). This is followed by a definition of Shamal events and related definitions used by other authors (Section 1.2). Section 1.3 summarizes the relevant

* Correspondence to: A. Anis, Marine Sciences & Oceanography, Texas A&M University, 200 Seawolf Parkway, Galveston, TX 77553, USA. E-mail: anisa@tamug.edu

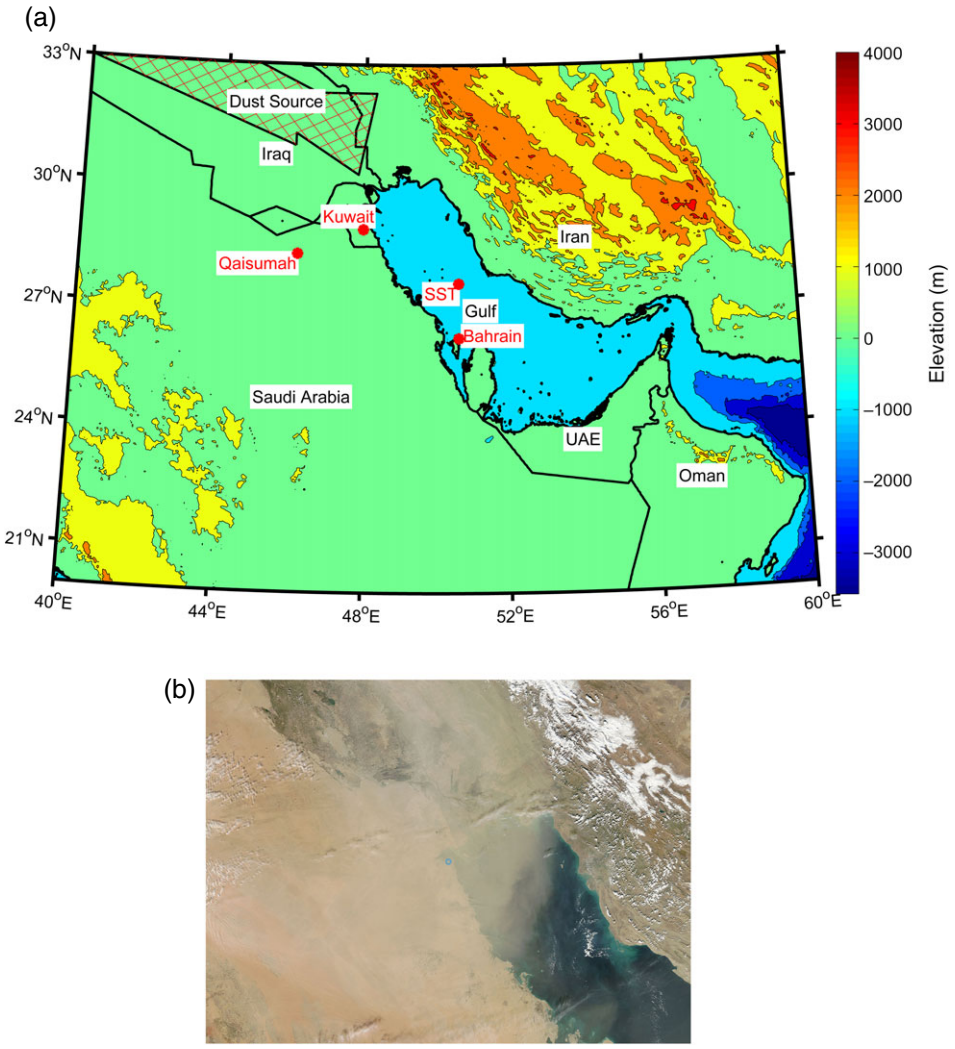

Figure 1. (a) Topographic map of the Gulf and the Mesopotamian dust source region (hatched) with the locations of the three meteorological stations and SST used in the study indicated by circles (red in online); (b) true colour aqua satellite image of N Gulf dust storm on 8 January 2013. The circle (blue in online) shows the location of Kuwait City (NASA, 2013).

background information on the three teleconnection patterns that are discussed in the paper. Observational and reanalysis data sources, as well as how various parameters were computed, are described in Section 2. Section 3.1 describes results and discusses the climate variability of the N Gulf region in the past 40 years in relation to teleconnection patterns as well as the meteorological and anthropogenic influences on visibility. The variability of Shamal events from 1973 to 2012 and their influence on meteorological parameters are described in Section 3.2. A short summary and conclusion is given in Section 4.

1.1. Climate characteristics

The Gulf is located in the subtropical high-pressure region, where the climate is classified as arid. The combination of high evaporation (1.4 m year^{-1}) (Privett, 1959) and low precipitation rates (0.03–0.11 m year^{-1}) (Almazroui *et al.*, 2012a) renders the ecosystem, and the society in particular, vulnerable to global warming effects.

The climate in the Gulf can be divided into two main seasons with two transition periods: summer season (Jun–Sep), fall transition (Oct–Nov), winter season (Dec–Mar), and spring transition (Apr–May) (Walters, 1990). During transition periods, weather is commonly unstable with no well-defined weather patterns, and tropical storms are common.

1.1.1. *Summer season*

Summer in the N Gulf is influenced by two main pressure systems. The first is the stationary summer monsoon low pressure system centred over NW India and extending W to the SE Gulf. The second is the stationary high pressure system over the E Mediterranean with a ridge extending SE towards the NW Gulf. These two systems produce a steep pressure gradient in between, which lies over the NE Gulf (Nasrallah *et al.*, 2004) and produces strong NW winds (7–13 m s^{-1}) (Bartlett, 2004) known as summer Shamals (Rao *et al.*, 2003); these may last up to weeks at a time (Wilkerson, 1991). The summer Shamals commonly

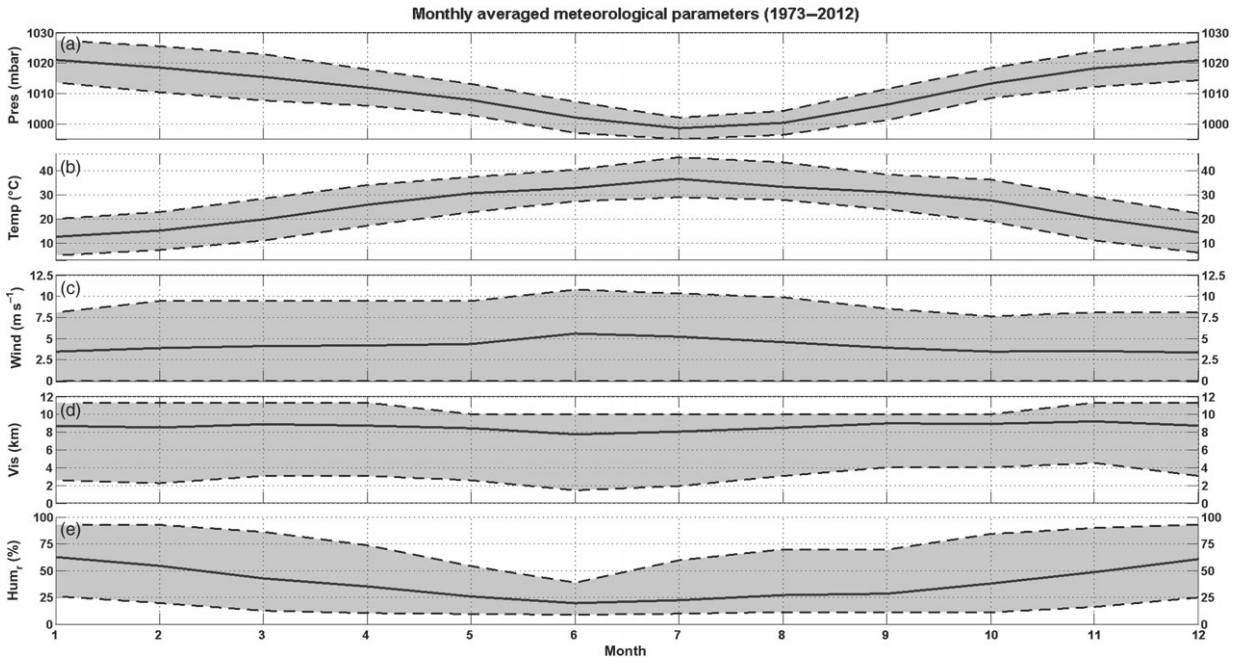

Figure 2. Monthly averaged (solid line) and range (shaded) of surface meteorological parameters (1973–2012): (a) barometric pressure, (b) air temperature, (c) wind speed, (d) visibility, and (e) relative humidity. (Data source: Kuwait Meteorological Office at Kuwait Airport station.)

bring dust or 'blazes' of hot (up to 51°C) and dry air called Simoom (literally meaning poison). The adiabatic ascent and descent of air passing the Zagros Mountains in NW Iran from the E results in extreme hot Simoom air. These conditions are common in the first part of summer (May–Jun), when the summer monsoon low is at its lowest.

From our analysis, the combination of high temperatures (average high 41°C), zero precipitation, and lower (550 $m^3 s^{-1}$) than yearly average (703 $m^3 s^{-1}$) river discharge from the Euphrates and Tigris (Janabi, 2010) during this period induces mineral crust formation, as shallow streams on the Mesopotamian floodplain (951,000 km^2) dry out (Partow, 2001). These processes, and the average high wind speeds (5.3 $m s^{-1}$) during this time of the year, contribute to rising dust formation making this period the lowest in visibility (8.1 km). Furthermore, a correlation of −0.83 (95% confidence interval of −0.51, −0.97) between wind speed and visibility suggests that winds are a major controlling factor of visibility throughout the year. Other characteristics of this period are relatively low barometric pressure (1000.4 mbar) and low relative humidity (21%) (Figure 2). The second part of summer (Jul–Aug) exhibits weakening, and eventually a breakdown of the summer monsoon low pressure system into two pressure systems centred over the SE Gulf and Iran. The weather in the N Gulf is controlled by the low pressure system in the SE (Nasrallah *et al.*, 2004) bringing about higher humidities (28%), weaker SE winds (4.2 $m s^{-1}$), and a slight increase in average visibility (8.7 km) (Figure 2).

1.1.2. Winter season

The winter season in the N Gulf is influenced by cold air carried into the region by the quasi-stationary Siberian high-pressure system in the E (Crook, 2009). This climate is often interrupted by frontal systems that build up in the E Mediterranean and move SE due to the upper-westerlies (Polar Front Jet). These moisture bearing frontal systems are the primary source of precipitation in the region (Barlow *et al.*, 2005). As the frontal system moves towards the Gulf, the Polar Front Jet behind the frontal system and the Sub-Tropical Jet ahead of it converge, strengthen the system, and generate strong winds at the front. On the passage of the front over the N Gulf, strong NW winds develop with fivefold the initial speed and reach values up to 15–20 $m s^{-1}$ near the surface at the centre of the Gulf (Thoppil and Hogan, 2010); these are known as winter Shamals. The duration of a winter Shamal event depends on how fast the upper air trough moves through the region, however, typical duration of a Shamal event is 2–5 days (Ali, 1994). From our analysis, the general characteristics of this period are: colder temperatures (15°C), higher relative humidity (55%), lower wind speed (3.7 $m s^{-1}$), higher barometric pressure (1019 mbar), and increased visibility (8.8 km) when compared to other periods throughout the year (Figure 2).

1.2. Shamal events

Dominating winds, referred to as Shamal winds, in the region are mainly from the N-NW throughout the year (Figure 3). These winds are sometimes interrupted by rare, more localized SE winds locally known as 'Kaus', lasting from a few hours to a few days (Chao *et al.*, 1992). Shamal winds can intensify well above the average and turn into what are considered 'Shamal events'. Topography of the region also plays a major role in strengthening the wind with the high terrain along the Iranian Coast (Zagros Mountains) and the W coast of Saudi Arabia (Figure 1)

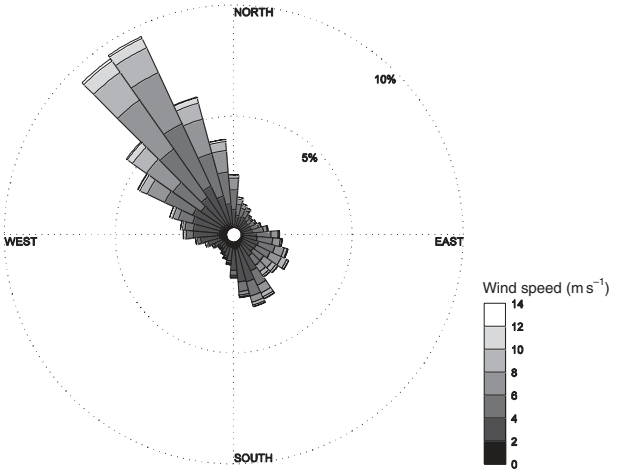

Figure 3. Hourly averaged wind speed, direction (from where wind blows), and frequency of occurrence (in %) during 1973–2012. (Data source: Kuwait Meteorological Office at Kuwait Airport station.)

producing a 'wind funnel' like structure (Giannakopoulou and Toumi, 2012). Commonly, Shamal events occur in the summer and winter seasons. Shamal events accompanied by rising dust originating from the Mesopotamian region (Iraq, E Syria, and SE Turkey) (Wilkerson, 1991) can lead to dust storms (Figure 1). The standard definition of dust storms is when visibility falls to $\leq$1 km because of dust (Kutiel and Furman, 2003; Goudie, 2009; Zhao *et al.*, 2010; Al-dousari and Al-awadhi, 2012).

Presently there is no agreed upon and clear definition of a Shamal event. Rao *et al.* (2001) define a Shamal event as a NW-N wind with an average speed of $\geq$8.75 m s^{-1} during at least 3 h of the day. Vishkaee *et al.* (2012) argue that for a Shamal to be characterized as an event five out of the six following conditions are to be met: (1) decrease in humidity, (2) decrease in surface temperature, (3) increase in barometric pressure, (4) Northerly winds, (5) wind speed >6 m s^{-1}, and (6) abrupt drop in visibility rate (3 km h^{-1}). Perrone (1979), the first known author to publish about Shamals, and Walters (1990) subdivide Shamal events into two types. The first is a short duration (24–36 h) event with NW winds $\geq$15.5 m s^{-1}, and the second is a long duration (3–5 days) event with NW winds up to 25.7 m s^{-1}. Next, we describe the operational definition of a Shamal event used in this study.

First, we note that associated with Shamal events is a reduction in visibility either due to rising dust or dust storms (visibility $\leq$1 km; Kutiel and Furman, 2003). We define a wind-speed threshold value required to lift dust into the air, based on the results of a comprehensive study by the US Army Natick Laboratories on wind borne dust in desert areas of various nature (sand dunes, desert flats, dry wash regions, desert pavements, alluvial fans, and playas). The study concluded that a speed of 9.85 m s^{-1} is required in a dry wash region to suspend dust into the air (Clements *et al.*, 1963). The Mesopotamian region is such a dry wash region that river streams are dry throughout most of the year. Furthermore, this threshold value is consistent with the range 8.95–11.18 m s^{-1} (UCAR/COMET, 2010) adopted by the Kuwait Meteorological Office and the United Nations Environment Programme (UNEP, 2013) for rising dust.

The operational definition of a Shamal day in this study is a WNW-N (287° < direction < 360°) wind with an hourly average speed $\geq$9.85 m s^{-1} blowing during at least 3 h day^{-1}. Two consecutive Shamal days are required for a Shamal to be classified as a Shamal event. Using two consecutive Shamal days to define an event is similar to the minimum number of days used by Reynolds (1993). Note that the condition of winds blowing for at least 3 h day^{-1} effectively filters out short duration wind events, such as sea-land breezes. Such breezes occur during more than 70% of the days in a year in this region and have wind speeds $\geq$10 m s^{-1} for less than 3 h day^{-1} (Eager *et al.*, 2008).

1.3. Teleconnection patterns

Various teleconnection patterns have been linked to the interannual variability in sea surface temperature (SST) (Saji *et al.*, 1999), air temperature (Philandras *et al.*, 2013), humidity (Dai, 2006), precipitation (Chang *et al.*, 2000), and also global warming (Cohen and Barlow, 2005) and droughts (Cullen and Demenocal, 2000). In this study we focus on the three teleconnection patterns: North Atlantic Oscillation (NAO), El Nino Southern Oscillation (ENSO), and Indian Ocean Dipole (IOD). These have been found in this study to have an influence on the N Gulf interannual barometric pressure, air temperature, and precipitation.

The NAO index is defined as the standardized difference between the sea level barometric pressure of the Azores high (station at Lisbon, Portugal) and Icelandic low (station at Reykjavik, Iceland) (Hurrell, 1995). The NAO peaks in its positive phase during the Northern Hemisphere winter season in response to the increased difference between air-sea temperatures (Cullen and Demenocal, 2000). A positive NAO phase results in a stronger subtropical high over the Azores that extends to the E Mediterranean and deepening of the Icelandic barometric low (Meehl and Loon, 1979). The ENSO index is defined as the area average of SST anomalies cross the E Equatorial Pacific (5°S–10°N, 150°W–90°W). The ENSO starts to develop in its positive phase during the months of Mar–Jun producing warmer SST's along the central Pacific Ocean as the trade winds weaken and tropical convection shifts E (Torrence and Webster, 1999). The shift of tropical convection and warming of the central Pacific Ocean SST causes disturbances to the Asian summer monsoon (Soman and Slingo, 1997), which controls the N Gulf summer season climate (details in Section 1.1). The IOD index is the standardized difference in SST between the W Indian Ocean (5°S–10°N, 50°E–70°E) and E Indian Ocean (10°S–0°S, 90°E–110°E) (Arun *et al.*, 2005). The change in trade winds direction from westerlies to easterlies produces warmer SST's in the W Indian Ocean and cooler SST's in the E Indian Ocean, which is similar to ENSO, also affects the Asian summer monsoon (Saji and Yamagata, 2003). The IOD starts to develop in its positive phase during the months of May–Jun (Saji *et al.*, 1999).

2. Methods

2.1. Data source

The observational dataset includes available hourly meteorological data of wind speed (Vaisala WS425 Ultrasonic), visibility (Vaisala FD12), barometric pressure (Vaisala PRB 100), and relative humidity (Vaisala HMP45D) and air temperature (Vaisala HMP45A) mounted in a radiation shield (Vaisala DTR503A) from 1973 to 2012 at the Kuwait Airport (29.242°N, 47.972°E, elevation 45 m; Figure 1), obtained from the Kuwait Meteorological Office (KMO). The sensors were set to take measurements once a minute and averaged and logged every 10 min. The 10-min data were then averaged over an hour. There were no major gaps in the dataset except from Aug/1990 to Jul/1991 due to the 1st Gulf War. The study was limited to 1973 as no observational hourly data prior to 1973 in the region was available. Furthermore, this dataset is unique since, to the best of our knowledge, no other dataset in the region has similar temporal resolution and detail. From this dataset, the variability in meteorological parameters over 40 years was estimated, as well as occurrence frequency of Shamal events. Other observational hourly datasets of temperature and barometric pressure at Qaisumah, Saudi Arabia (KSA) (28.335°N, 46.125°E, elevation 357 m; Figure 1) and Bahrain International Airport (BAH) (26.271°N, 50.634°E, elevation 1 m; Figure 1) available from the National Oceanic and Atmospheric Administration-National Climatic Data Center (NOAA-NCDC) from 1973 to 2012 were used in addition to the KMO data to analyze climate variability. Because of the very limited temporal resolution, continuity, and quality of precipitation data at the BAH and KSA stations, only the KMO precipitation data were used for analysis.

2.2. Climate variability

Yearly averages (1973–2012) and 95% confidence intervals of observed meteorological parameters was computed using the bootstrap method (Efron and Tibshirani, 1986). A linear fit to the yearly averaged data (e.g. Yosef *et al.*, 2009; Philandras *et al.*, 2013) were computed using the robust regression method (Huber and Ronchetti, 2009). From the fitted slope, changes in meteorological parameters, as well as changes in Shamal event occurrence frequency over the study period were estimated.

The effect of teleconnection patterns on the Gulf were generally more pronounced seasonally (winter: Dec–Mar and summer: Jun–Sep) than annually (more details in Section 1.3). Therefore, we focus on interannual seasonal variability in meteorological parameters to quantify the variability of a specific season in reference to the 40-year average. We define

$$\text{Interannual seasonal variability} = y - \overline{y}, \tag{1}$$

where y is a seasonal average of an observational meteorological parameter (e.g. air temperature) and its 40-year seasonal average is noted with an overline. The interannual seasonal variability was then standardized (Equation (2)), in a similar approach to that taken by Philandras *et al.* (2013) and Saji and Yamagata (2003), who analyzed the influence of teleconnection patterns on meteorological parameters over the E Mediterranean and Indian Ocean, respectively. Thus

$$z = \frac{y - \overline{y}}{\sigma}, \tag{2}$$

where z is the standardized interannual seasonal anomaly of an observational meteorological parameter y, and σ is the 40-year standard deviation. Spatial anomalies were computed from NCEP reanalysis (for details see Kanamitsu *et al.*, 2002) meteorological data at 6-h intervals and global coverage at a resolution of 1.875°. Spatial anomaly charts of meteorological parameters were constructed to assess the linkage between climate variability and teleconnection patterns.

To investigate the relation between the teleconnection patterns and meteorological anomalies, two goodness of fit statistics were computed. The first method is the Nash–Sutcliffe coefficient of efficiency (N_s; Nash and Sutcliffe, 1970) that determines how good the plot of the standardized teleconnection patterns indices *versus* the standardized meteorological anomalies fits the 1:1 line:

$$N_s = 1 - \frac{\sum_{i=1}^{n} \left(z_i - x_i\right)^2}{\sum_{i=1}^{n} \left(z_i - \overline{z}\right)^2}, \tag{3}$$

where x represents the standardized teleconnection pattern seasonal index, i is the yearly seasonal data point index, and n is the total number of years. The values of N_s range between $-\infty$ to $+1$, with 1 indicating a perfect relation, $N_s = 0$ indicating that the standardized meteorological seasonal anomaly is only as good as the standardized teleconnection pattern seasonal index average and $N_s < 0$ indicating a weak relation (Elsanabary and Gan, 2013). Generally, values between 0 and 1 are viewed as acceptable (Gupta and Kling, 2011). The second method used is the Pearson correlation defined as:

$$r = \sum_{i=1}^{n} \frac{\left(x_i - \overline{x}\right)\left(z_i - \overline{z}\right)}{(n-1)\,\sigma_x \sigma_z}, \tag{4}$$

where the value of r ranges between -1 and 1, with $r = 1$ and $r = -1$ indicating a perfect relation, and $r = 0$ indicating a poor relation. This method assesses the degree of collinearity between the standardized teleconnection patterns seasonal indices and the standardized meteorological parameter seasonal anomalies. Furthermore, this method was tested for significance (P_{value}) using the student's t-test with a critical value of 0.05 (Press *et al.*, 2007). Pearson correlations were used by Donat *et al.* (2014) when linking teleconnection patterns to the extreme changes in temperature and precipitation in the Middle-East.

For the indices of NAO, ENSO, and IOD, we used the monthly available data provided by NOAA Climate

Prediction Center (CPC) and the Japanese Agency for Marine-Earth Science and Technology (JAMSTEC) from 1973 to 2010. These data are based on the standardized (1970–2010 base period) latitudinal sea level pressure differences for NAO (Barnston and Livezey, 1987), and on the standardized longitudinal SST differences for ENSO and IOD (Saji *et al.*, 1999) (see further details in Section 1.3). These three (NAO, ENSO, and IOD) monthly indices have been further averaged over 3 months (seasonal average) to be consistent with our observational datasets (KMO, KSA, and BAH). This is similar to the approach used by Donat *et al.* (2014) and Elsanabary and Gan (2013) to examine the interannual seasonal variability of temperature and precipitation. Furthermore, the longest spatial available dust dataset for the study region was obtained from GEMS (Global and regional Earth-system Monitoring using Satellite and *in-situ* data, Hollingsworth *et al.*, 2008) developed by ECMWF-IFS (European Centre for Medium-Range Weather Forecasts-Integrated Forecast System, Benedetti *et al.*, 2009) between 2003 and 2012 in the form of Dust Aerosol Optical Depth at 550 nm (DU). This data is derived from the reanalysis of four-dimensional variational (4D-Var) aerosol assimilation using a combination of satellite-based (Moderate Resolution Imaging Spectroradiometer-MODIS) and background meteorological data such as wind at 10 m to forecast the dust distribution and trajectory (Morcrette *et al.*, 2008). The observational DU from MODIS is determined using the dusts specific physical and optical properties (mass extinction, α_{ei}, single scattering albedo, ω, and asymmetry factor, g; see Appendix) at a wavelength, λ, of 550 nm (Reddy, 2005) by

$$\mathrm{DU} = \sum_{i=1}^{n} \int_{Pres}^{0} \alpha_{ei}\left(\lambda, Hum\left(Pres\right)\right) r_i\left(Pres\right) \frac{dp}{g} \quad , \qquad (5)$$

where n is the number of dust aerosols, *Pres* is the surface pressure, *Hum* is the relative humidity, r is the mass mixing ratio, and dp is the model layer pressure (Benedetti *et al.*, 2009). The 10-year DU spatial dataset was used to compare the variability of the observed visibility data and to investigate the controlling factors (anthropogenic activity and meteorological parameters) that may have led to fluctuations in the interannual variability of DU.

2.3. Metrics of Shamal effects

The influence of Shamal events on meteorological parameters during 1973–2012 is determined by quantifying both average and extreme parameter values of the difference between pre-Shamal (a day before Shamal) to Shamal event conditions. These are summarized in the following equations and are based on wind speed (Equations (6) and (7)), visibility (Equations (8) and (9)), air temperature (Equations (10) and (11)), relative humidity (Equations (12) and (13)), and barometric pressure (Equations (14) and (15)):

$$\Delta Wind_{\mathrm{avr}} = \text{Shamal average } Wind - \text{pre-Shamal average } Wind, \qquad (6)$$

$$\Delta Wind_{\max} = \text{Shamal hourly max } Wind - \text{pre-Shamal hourly max } Wind, \qquad (7)$$

$$\Delta Vis_{\mathrm{avr}} = \text{Shamal average } Vis - \text{pre-Shamal average } Vis, \qquad (8)$$

$$\Delta Vis_{\min} = \text{Shamal hourly min } Vis - \text{pre-Shamal hourly min } Vis, \qquad (9)$$

$$\Delta Temp_{\mathrm{avr}} = \text{Shamal average } Temp - \text{pre-Shamal average } Temp, \qquad (10)$$

$$\Delta Temp_{\max} = \text{Shamal hourly max } Temp - \text{pre-Shamal hourly max } Temp, \qquad (11)$$

$$\Delta Hum_{\mathrm{r\ avr}} = \text{Shamal average } Hum - \text{pre-Shamal average } Hum, \qquad (12)$$

$$\Delta Hum_{\mathrm{r\ max}} = \text{Shamal hourly max } Hum - \text{pre-Shamal hourly max } Hum, \qquad (13)$$

$$\Delta Pres_{\mathrm{avr}} = \text{Shamal average } Pres - \text{pre-Shamal average } Pres, \qquad (14)$$

$$\Delta Pres_{\max} = \text{Shamal hourly max } Pres - \text{pre-Shamal hourly max } Pres, \qquad (15)$$

where *Wind* is wind speed, *Vis* is visibility, and *Temp* is air temperature.

3. Results and Discussion

3.1. Climate variability in the N Gulf (1973–2012)

The increase of carbon dioxide (from 280 to 390 ppm; Blasing, 2013) and other greenhouse gases due to the burning of fossil fuels since the industrial revolution (1750) has led to a pronounced increase in global temperature (Preining, 1992) of 0.4–0.8°C during the past century (EPA, 2012). Our analysis suggests that the temperature in the N Gulf has increased by 0.8°C just in the past 40 years and may continue to increase at a rate of 0.02°C year^{-1} (0.01, 0.04) if we assume a similar trend of increase in air temperature (Figure 4(a)). This is lower compared to the

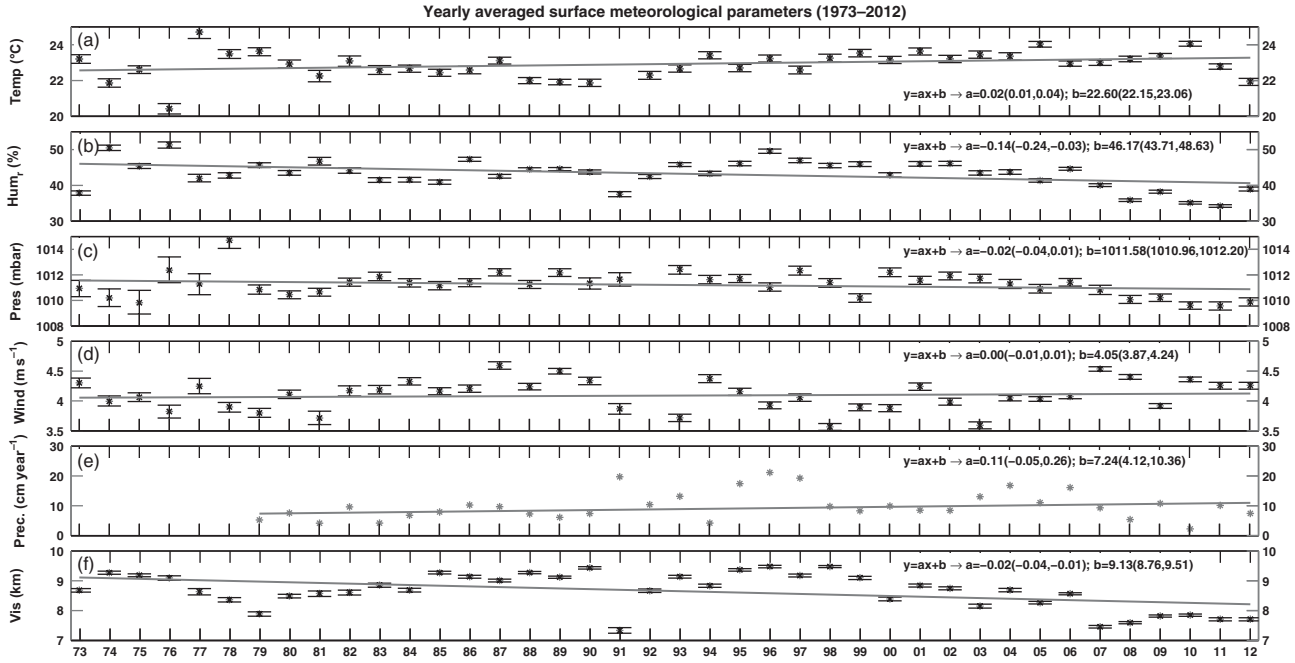

Figure 4. Yearly averaged surface meteorological parameters observed at KMO from 1973 to 2012 and their 95% bootstrap confidence interval error bars. A linear fit to the data, using robust regression is represented by the solid lines: (a) air temperature, (b) relative humidity, (c) barometric pressure, (d) wind speed, (e) precipitation, and (f) visibility.

average 0.06°C year^{-1} across Saudi Arabia (27 observational sites) reported by Almazroui *et al.* (2012b) between 1979 and 2009. Moreover, a previous study by Nasrallah and Balling (1995) reported large variations (−0.09 to 0.07°C decade^{-1}) in temperature trends at three locations in Saudi Arabia (30°N, 40°E; 25°N, 50°E; 20°N, 40°E), using an updated version of gridded points created by Jones *et al.* (1986) between 1950 and 1990. Nasrallah and Balling (1995) linked 30% (correlation of 0.55) of the temperature trend variances in Saudi Arabia as well as the Middle East to anthropogenic induced desertification. Air surface temperature plays a major role in influencing other meteorological parameters such as humidity and barometric pressure. Although air at higher temperatures can contain more water vapour (Hansen *et al.*, 1984), observed humidities were not higher in the N Gulf region. The relative humidity level has dropped by 6% between 1973 and 2012 (Figure 4(b)), in agreement with climate models that show a similar decrease in humidity in the Middle East as a result of global warming (Dai, 2006). Another meteorological parameter impacted by global warming in the N Gulf is barometric pressure. The increase of land and SST's following the increase in near surface air temperature results in increased loss of longwave (infrared) radiation from the land and sea bodies, contributing to a reduction in barometric pressure by an overall of 0.8 mbar (0.02 mbar year^{-1}) between 1973 and 2012 (Figure 4(c)). The decrease in barometric pressure reported in this study is similar to that reported by El Kenawy *et al.* (2012), whose study suggested a decrease of 0.02 mbar year^{-1} between 1920 and 2006 for the W Mediterranean region.

Barometric pressure and surface air temperature were found to fluctuate throughout the study period in response to the NAO and ENSO teleconnection patterns. A previous study by Cullen and Demenocal (2000), used monthly air temperature and precipitation observations at 770 stations, extending from the Iberian Peninsula to the Middle East (20°N–50°N and 10°W–50°E), to construct yearly winter season temperature and precipitation anomaly indices from 1930 to 1995 and link these to the NAO index. Their study suggests that the effect of a positive NAO phase during winter extends to the Mesopotamian region causing cooler temperatures by 18% (correlations of −0.42) and a reduction in precipitation of 27% (correlations of −0.52). Similarly, a study by Donat *et al.* (2014) used 61 observational stations measuring daily air temperature and precipitation across the Arab region, including two of the three stations used in the present study (KIA and BAH), and suggests a correlation of −0.2 between winter air temperatures and NAO for the N Gulf region from 1961 to 2010. These conditions are a result of the Azores High and Icelandic Low shifting the moisture bearing Jet Stream poleward and bringing wetter and warmer conditions to N Europe and cooler and drier conditions to the Mediterranean and Mesopotamian regions (Chang *et al.*, 2000; Cullen and Demenocal, 2000), thus providing a possible link of precipitation, air temperature, and barometric pressure in the Mesopotamian region to the NAO. The observational results reported here for the winter seasons of 1973–2012 in the N Gulf are consistent with those of Cullen and Demenocal (2000) and Donat *et al.* (2014) for the Mesopotamian region and suggests that the winter barometric pressure anomalies (Figure 5(a)) and air temperature anomalies (Figure 5(e)) in the N Gulf are impacted by the NAO with positive N_s values and significant ($p_{\text{value}} < 0.05$) correlation values

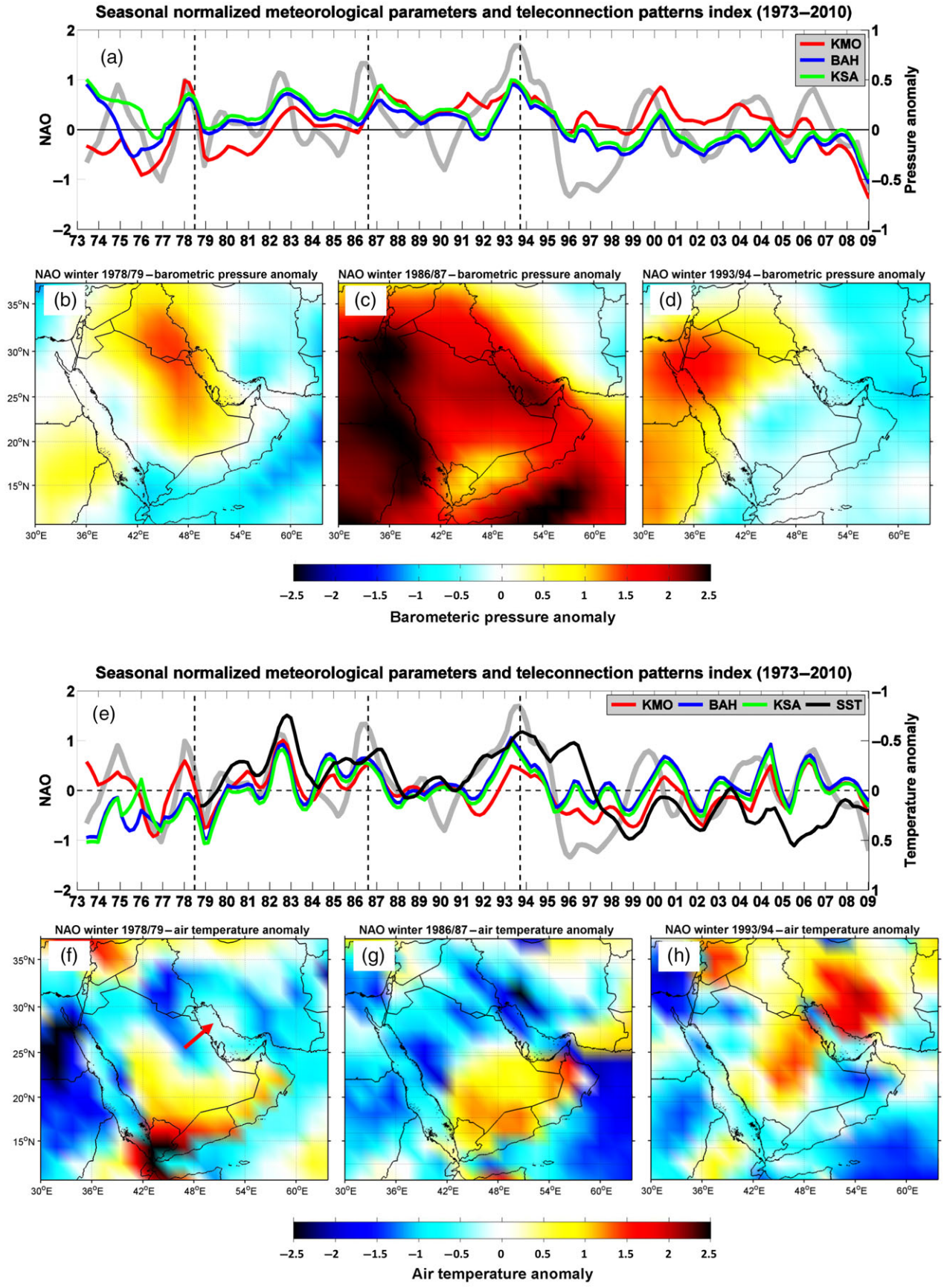

Figure 5. (a) Winter averaged NAO index (grey) and winter barometric pressure anomalies (Equation (2); KMO; BAH; KSA). Vertical broken lines indicate strong (index ≥1) positive NAO phases. (b–d) Winter barometric pressure anomalies computed as in Equation (2) using NCEP barometric pressure data. (e–h) similar to (a–d) but for air temperature anomalies.

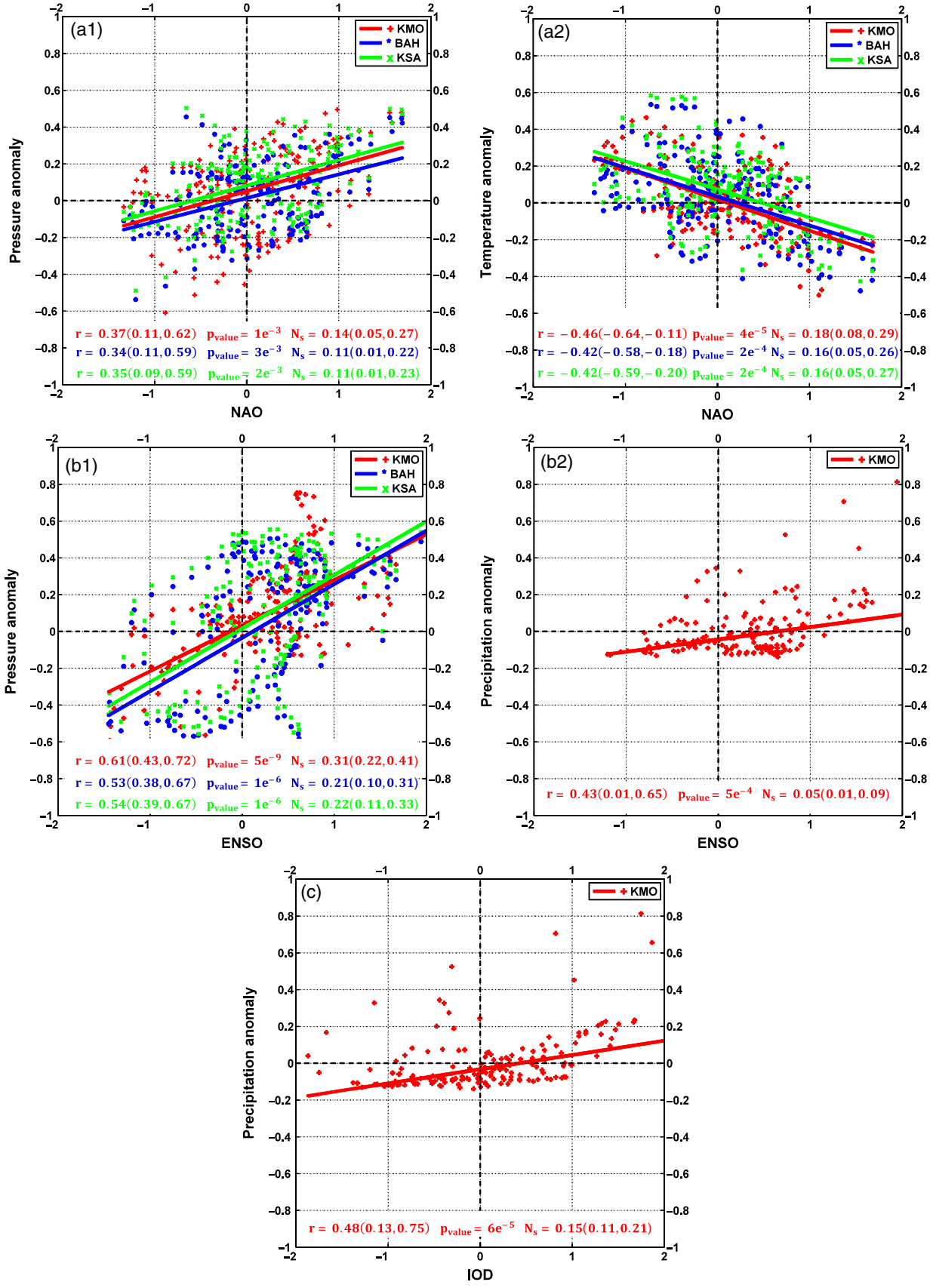

Figure 6. Seasonal averaged teleconnection patterns indices versus meteorological parameters anomalies (1973–2012) scatter plots at KMO, BAH, and KSA, with their respective correlations, *p*-values, and Nash–Sutcliffe coefficient. A linear fit to the data, using robust regression is represented by the solid lines: (a1) NAO index versus barometric pressure anomaly observations, (a2) NAO index versus air temperature anomaly observations, (b1) ENSO index versus barometric pressure anomaly observations, (b2) ENSO index versus precipitation anomaly observations, and (c) IOD index versus precipitation anomaly observations.

ranging from 0.34 to 0.37 and −0.42 to −0.46, respectively (Figure 6(a)).

The impact of strong (index ≥1) NAO positive periods (1978/79, 1986/87, and 1993/94; Figure 5(a) and (e)) have caused relative higher winter barometric pressure and cooler surface air temperatures by up to 2.8 mbar (0.4%) and −2.4°C (−22%), respectively (Table 1). Furthermore, the strong NAO positive index (≥1) periods were examined spatially for winters 1978/79, 1986/87, and 1993/94 barometric pressure anomalies and temperature anomalies (Figure 5(b)–(d) and (f)–(h)). The barometric spatial anomaly results show a positive anomaly extending from NE Africa towards the N Gulf in winters of 1978/79 and 1993/94 (Figure 5(b) and (d)) and at times covering all the Gulf in winter 1986/87 (Figure 5(c)). The spatial air temperature anomalies (Figure 5(f)–(h)) followed a similar pattern to that of barometric pressure anomalies with negative anomalies extending from NE Africa towards the N Gulf. An exception was during the 1978/79 winter when the temperature anomaly at BAH and KSA was ∼0 compared to the negative anomaly of −1 at KMO (Figure 5(e)). This may be explained by the negative air temperature anomaly centred over the Gulf (indicated by the red arrow Figure 5(f)) and not extending to Kuwait. Moreover, possible connection between NAO and SST was quantitatively explored using the SST anomalies computed from the NCEP SST reanalysis data for the period 1979–2010 at a location centred in the N Gulf region (Figure 1). During positive NAO phases SST anomalies were found to decrease, following a similar pattern to that of air temperature (Figure 5(e)). Further analysis revealed a consistent lag of SST behind NAO, suggesting a delayed response of SST to NAO of about 1 month compared to the relatively immediate response of air temperature. The influence of the NAO on the variability in precipitation reported by Cullen and Demenocal (2000) has not been observed in our KMO dataset.

Similar to the NAO, ENSO is another large scale mode of climate variability (Jin, 2003). Of particular importance to the present study region is the weakening of the summer monsoon during positive phase ENSO events. During these events, the tropical convection shifts eastward causing a weaker low pressure monsoon over India, which in turn induces a disturbance to the Jet Stream (Shakula and Paolino, 1983; Joseph *et al.*, 1994; Webster, 1995; Webster *et al.*, 1998). It is of interest to note that the impact of ENSO on the summer monsoon (barometric pressure, air temperature, and precipitation) was first introduced by (Walker and Bliss, 1937). The disturbance to the low pressure summer monsoon during the three analyzed ENSO events (1982, 1987, 1997; Table 1) was observed to result in higher barometric pressure (up to 1.6 mbar (0.02%) in summer 1997; Table 1) and an increase in precipitation (up to 4.5 cm month^{-1} (31%) in summer 1997; Table 1). The increase in their respective anomalies is shown in Figure 7(a) and (e). Correlation values between barometric pressure anomalies and ENSO index ranged between 0.53 to 0.61 and the correlation value of

Table 1. Interannual seasonal variability of meteorological parameters (Equation (1)) at the KMO during teleconnection pattern events.

	Event year	ΔPressure [mbar]	ΔTemperature [°C]	Tele. index
NAO	1978/79 Winter	2.8 (1.8,3.8)	−2.4 (−3.2,−1.5)	1.0
	1986/87 Winter	1.4 (1.1,1.6)	−1.5 (−1.7,−0.9)	1.1
	1993/94 Winter	2.3 (1.7,2.9)	−1.6 (−2.0,−1.3)	1.7
		ΔPressure [mbar]	ΔPrecipitation [cm month^{-1}]	
ENSO	1982 Summer	0.6 (0.6,0.7)	1.3 (1.2,1.6)	1.6
	1987 Summer	1.1 (1.0,1.2)	0.9 (0.8,1.2)	1.7
	1997 Summer	1.6 (1.5,2.1)	4.5 (4.3,5.3)	2.3
		ΔPrecipitation [cm month^{-1}]		
IOD	1982 Summer	1.3 (1.2,1.6)		1.4
	1994 Summer	1.4 (1.1,1.6)		1.7
	1997 Summer	4.5 (4.3,5.3)		2.3

95% bootstrap confidence intervals are given in parentheses.

precipitation anomalies and ENSO index was 0.43, with positive N_s values suggesting a significant ($p_{\text{value}} < 0.05$) relation between these parameters and the ENSO event (Figure 6(b)). Spatial anomaly results for barometric pressure during ENSO events show positive anomalies extending from the Arabian Sea and W India towards the Gulf (Figure 7(b)–(d)). Spatial anomaly results for precipitation (Figure 7(f)–(h)) show a scatter of positive anomalies over the Gulf region covering Kuwait, United Arab Emirates, Oman, and parts of Saudi Arabia and Qatar. Similar conclusions for the influence of ENSO on the increase of regional precipitation have been observed by Kumar and Ouarda (2014) and Arun *et al.* (2005). Both studies found correlations >0.4 between precipitation values and ENSO index using monthly observations at six sites located in the United Arab Emirates between the years 1981–2011 (Kumar and Ouarda, 2014) and NCEP reanalysis data across Saudi Arabia between 1958 and 2012 (Arun *et al.*, 2005). The increased precipitation due to ENSO appears to be in contrast to the observations of Donat *et al.* (2014) for the N Gulf, whose study suggests a weak relation between winter precipitation and ENSO for the period of 1961 to 2010. We suggest that the effect of ENSO on the regional precipitation is a result of its influence on the summer monsoon, thus, influencing the N Gulf during summer when the monsoon reaches its highest latitude and therefore is closest to the N Gulf (see further details in Section 1.1). Furthermore, the largest summer precipitation (4.5 cm month^{-1}, 31%) in the N Gulf was observed in 1997, when the strongest ENSO event was recorded (Jin, 2003).

During 1997 the IOD was also in a strong (index ≥1) positive phase. During a positive IOD event the E Indian Ocean becomes relatively colder, while the W Indian Ocean becomes relatively warmer. These unusual temperature conditions suppress atmospheric convection in the E Indian Ocean, while enhancing atmospheric convection

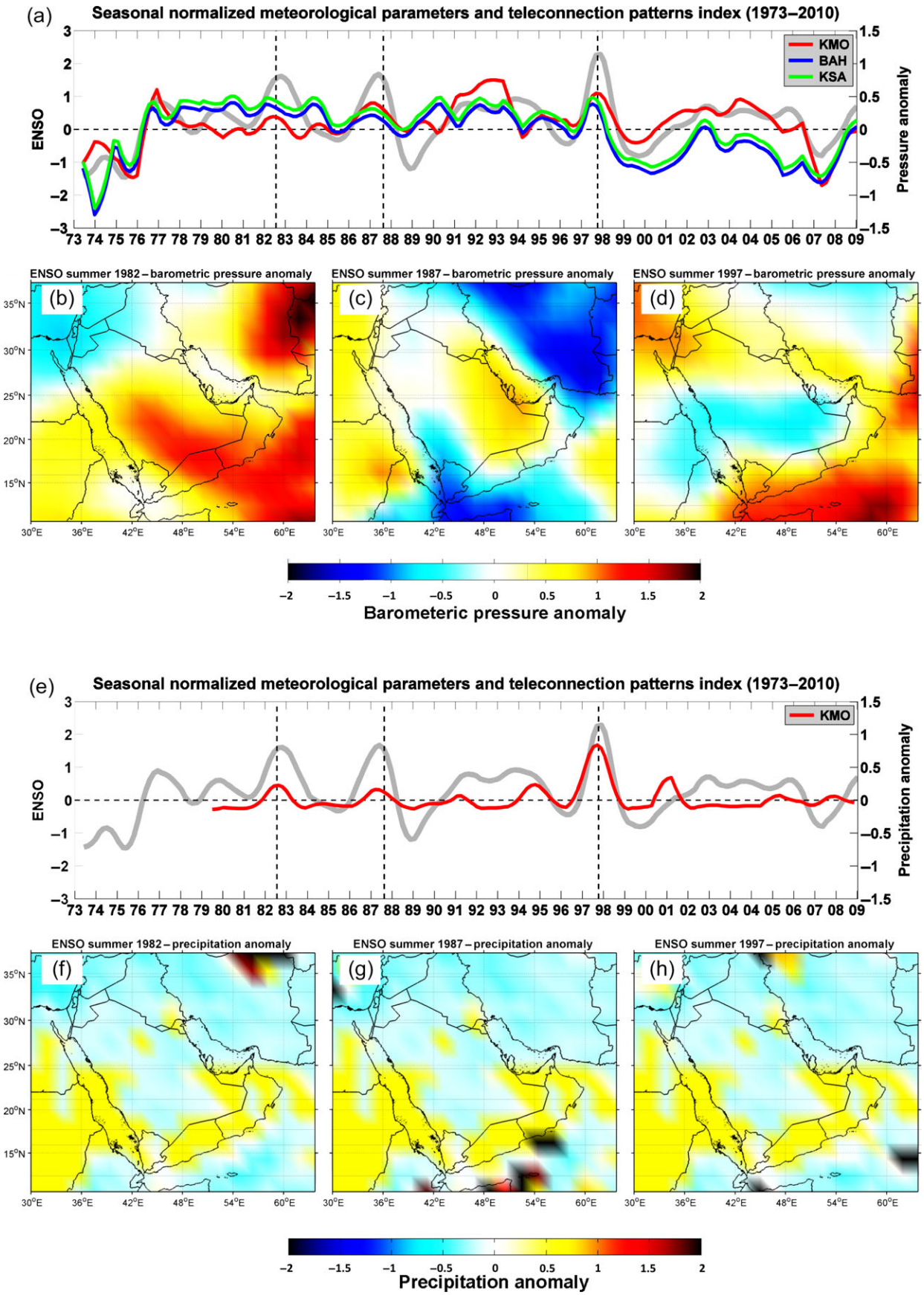

Figure 7. (a) Summer averaged ENSO index (grey) and summer barometric pressure anomalies (Equation (2); KMO; BAH; KSA). Vertical broken lines indicate strong (index ≥1) positive ENSO phases. (b–d) Summer barometric pressure anomalies computed as in Equation (2) using NCEP barometric pressure data. (e–h) are similar to a–d but for precipitation anomalies.

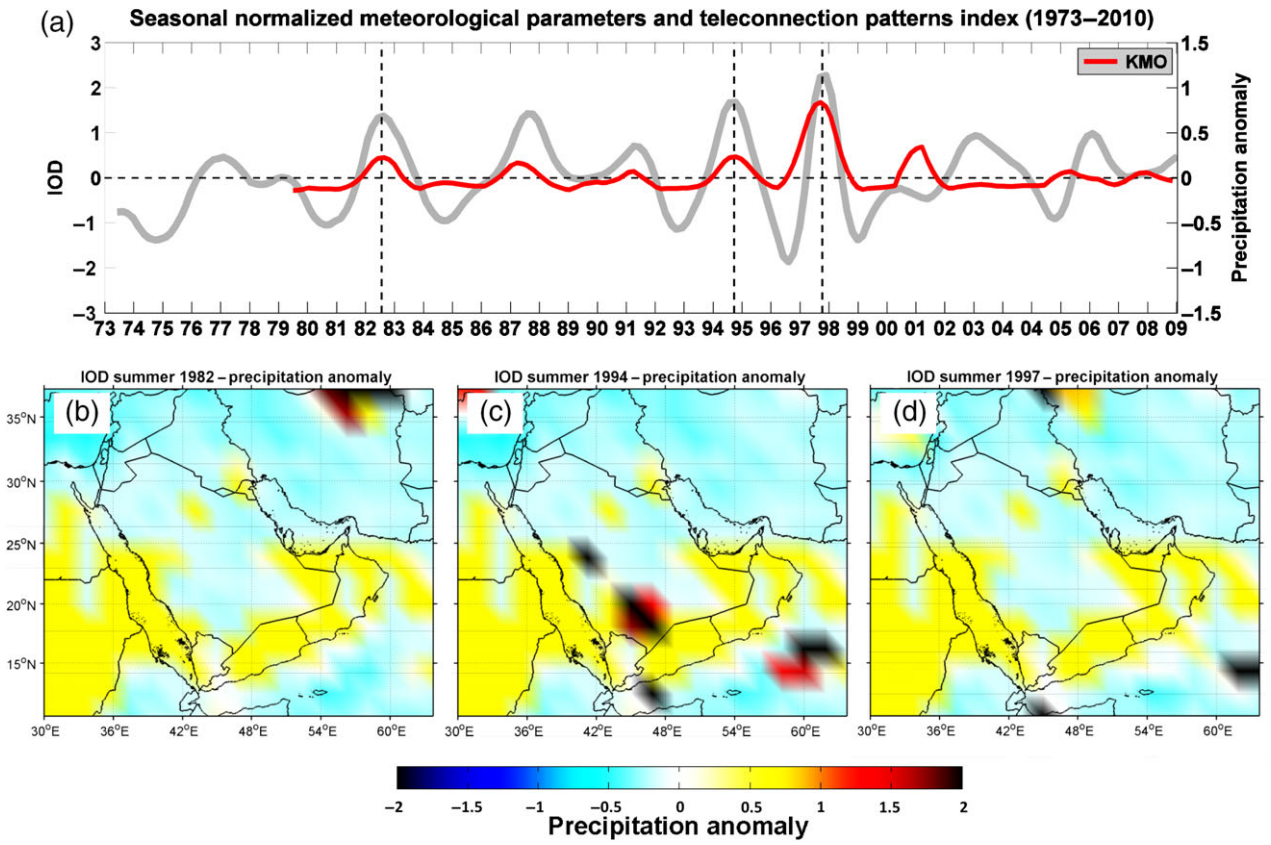

Figure 8. (a) Summer averaged IOD index (grey) and summer precipitation anomalies (Equation (2); KMO). Vertical broken lines indicate strong (index ≥1) positive IOD phases. (b–d) Summer precipitation anomalies computed as in Equation (2) using NCEP precipitation data.

in the W Indian Ocean. This impacts the Indian summer monsoon low pressure system (Saji *et al.*, 1999) causing an increase in precipitation over the W Indian Ocean region (Goes *et al.*, 2005). An increase in precipitation was observed during the 1982, 1994, and 1997 summer events (Figure 8(a)–(d); Table 1). Furthermore, the correlation between precipitation and the IOD index was 0.48, with a positive N_s value suggesting a significant ($p_{\text{value}} < 0.05$) relation between the two (Figure 6(c)). Similarly, a study by Webster *et al.* (1999) suggests a strong correlation (0.62) between E African precipitation and the IOD, based on NCEP reanalysis SST and upward longwave radiation (as a proxy for precipitation) for 1997–1998 across the Indian Ocean, when compared to 40 year observational climate variability in the region. On the basis of these results, Webster *et al.* (1999) suggests that during IOD events the precipitation over the W Indian Ocean region is above average and below average over the E Indian Ocean region.

The controlling factor of visibility in the Gulf is dust, with fog being uncommon. The DU data (Figure 9) was found to be significantly ($p_{\text{value}} < 0.05$) correlated to the KMO visibility data (Figure 4(f)) with a value of 0.76 (0.30, 0.93), suggesting dust to be indeed a main controlling factor of visibility.

For dust to be lifted into the air a lifting force is required and is commonly supplied by the action of the wind. Another important factor controlling the amount of dust lifted into the air is related to the state and properties of the land surface, e.g. dry vs wet desert surface. During the last 10 years of the dataset (2003–2012), the DU has fluctuated in response to the wind strength and local precipitation (Figure 10), such that the relative increase in precipitation and reduction in wind speed resulted in lower DU. However, in 2003 the above (31%) than 40 year average in precipitation and lower (11%) than 40 year average in wind speed did not result in relatively lower observed DU as for other years (Figure 10). This may suggest other contributing factors. A previous study by Koch and El-Baz (1998) outlines the changes between pre- and post-war desert conditions (Iran–Iraq War in 1980–1988 and 1st Gulf War in 1990–1991) and suggests that military activities have changed desert morphology and environmental conditions of 22% of the desert areas. These morphological changes are mainly a result of disturbances caused to the desert pavement layer, which protects sand particles from exposure to wind erosion, leading to weaker pick-up wind speeds required to suspend dust into the air. Based on the above, we are led to suggest that environmental changes in desert morphology, possibly related to 'Operation Iraqi Freedom' in 2003, may have lead to the observed increase in DU in 2003. Furthermore, a case study by Saeed *et al.* (2014) during 'Operation Iraqi Freedom' suggested an increase in dust storm intensity in the N Gulf as a result of military activity.

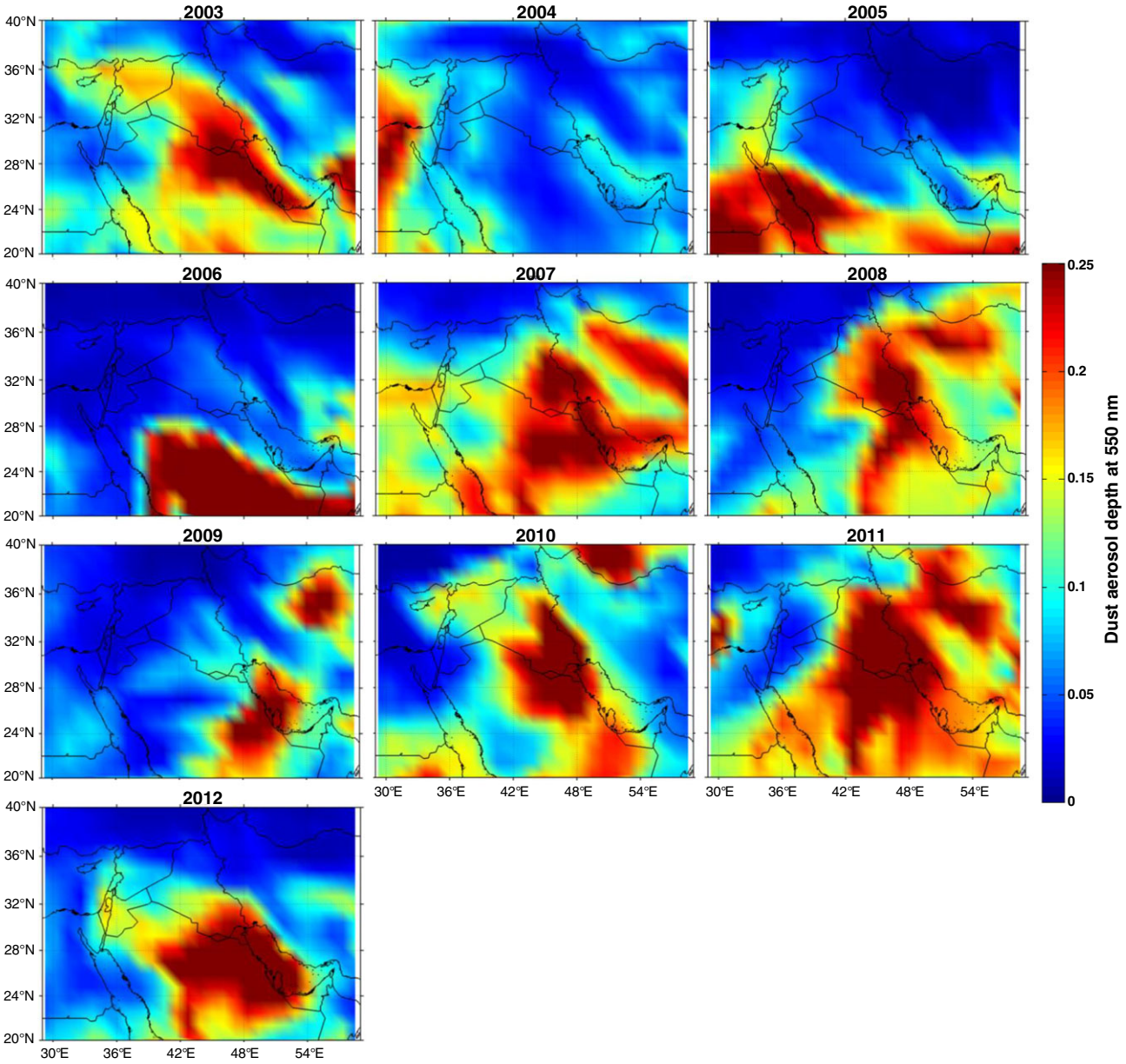

Figure 9. Yearly averaged (2003–2012) dust aerosols optical depth at 550 nm (unitless; represents the fraction of light that is not scattered or absorbed; Chin *et al.*, 2002).

3.2. Shamals

3.2.1. Effects of Shamal events on meteorological parameters

Development of N-NW winds during Shamal events between 1973 and 2012 (Figure 11) showed an average increase in wind speed of 2.7 m s^{-1} (Figure 12(a), Table 2). Average wind speeds of 11.5 m s^{-1} (7.2, 15.2) with maximum wind speeds up to 23 m s^{-1} were registered during these events. Similar observed wind speed averages have been reported by Rao *et al.* (2001), who used hourly wind speed/direction at Doha, Qatar, between 1990 and 2000. However, these average wind speeds are lower than the reported wind speeds ($\geq$15.5 m s^{-1}) by Walters (1990) (Section 1.2).

Average wind speeds during Shamal events that were higher than the dust pick-up threshold speed (9.85 m s^{-1}) reduced visibility by an average of 1.7 km (Figure 12(b), Table 2), resulting in average visibilities of 4.3 km (0.6, 9.0) as dust was being suspended into the air from the Mesopotamian region (Figure 1). Shamal winds brought drier air to the region while travelling over the continental land mass, reducing the relative humidity by 4.3% on average (Figure 12(c), Table 2).

Changes in barometric pressure during Shamal events (Figure 12(d)) were dependent on the season. In the winter, a cold frontal system moving from the E Mediterranean and the development of a high pressure system over Iraq, Kuwait, and Saudi Arabia generates steep pressure gradients leading to winter Shamals (Thoppil and Hogan, 2010).

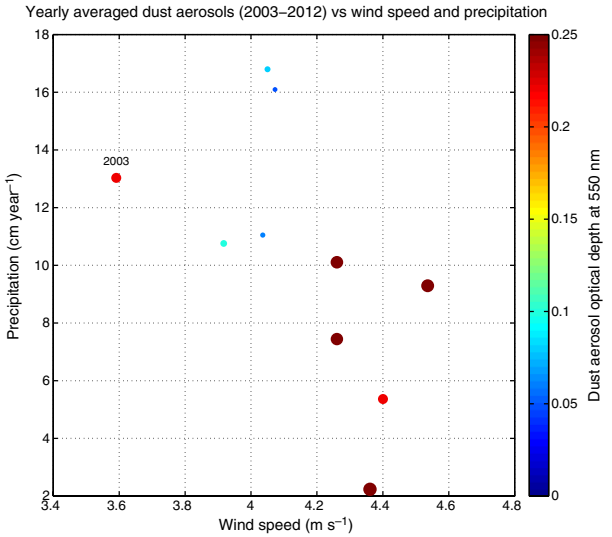

Figure 10. Yearly averaged (2003–2012) dust aerosols (coloured circles) at Kuwait versus wind speed (horizontal coordinate) and precipitation (vertical coordinate). Colours and size of data points represent the quantitative measure of the dust aerosols optical depth at 550 nm (unit less).

The development of a high pressure system during winter Shamals causes an average increase in barometric pressure of 7.8 mbar (Figure 13(d), Table 3). This increase in barometric pressure during winter Shamals is in agreement with Vishkaee *et al.* (2012) case study on 22–23 February 2010, which used 13 observational land sites (8 in Iraq and 5 in Iran) and ECMWF reanalysis for analysis. In summer, the stationary summer monsoon low pressure system over NW India, which affects the N Gulf region, induces the summer Shamal and reduces the barometric pressure by an average of 0.6 mbar (Figure 13(d), Table 3) during Shamal events.

The change in air temperature (Figure 12(e)) during Shamal events was also dependent on the season. Winter Shamals resulted in a reduction of temperatures by 1.5°C, while summer Shamals resulted in an increase of 0.8°C (Figure 13(a), Table 3). Overall, with exception of air temperature and barometric pressure, there was no significant difference between summer and winter Shamals and average differences of visibility, humidity, and wind speed were similar in both seasons (Figure 13, Table 3). By comparing the differences in meteorological parameters due to Shamal events, it is apparent that winter Shamals exhibited larger variability than summer Shamals, as indicated by the larger standard deviation values of the differences in meteorological parameters (Table 3). The SE 'Kaus' wind that travels over the Gulf prior to winter Shamals (Figure 11(d)) is suggested to be the main reason for the larger variability in relative humidity and air temperature, as the 'Kaus' wind brings humid and warmer conditions during pre-Shamal.

3.2.2. *Variability of Shamal events (1973–2012)*

A total of 1165 days, comprised of 421 Shamal events (281 summer, 57 winter, and 83 transition periods), occurred during the study period (1973–2012) with the number of Shamal days per year fluctuating throughout this period. The average number of Shamal days and events stands on 29 days year^{-1} and 10 events year^{-1}, respectively. 1973

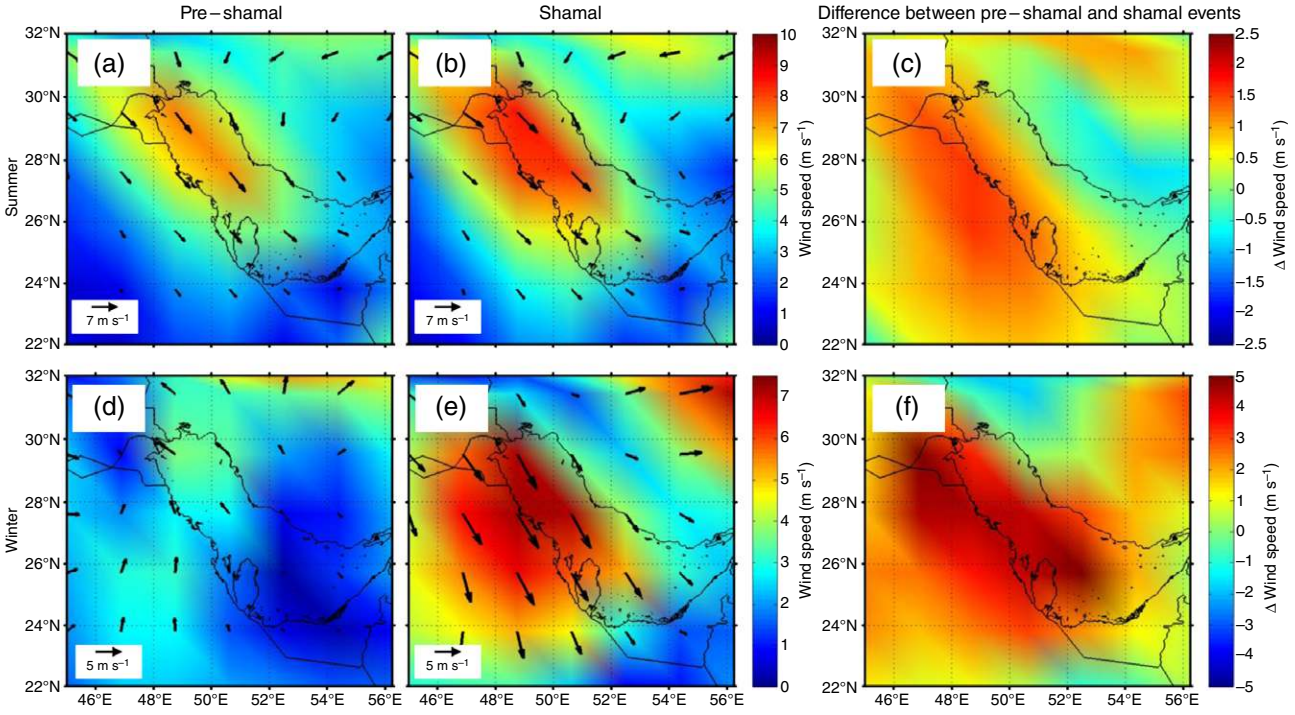

Figure 11. Differences in wind speeds (Equation (6)) between pre-Shamal and Shamal events (1973–2012): (a) average wind speeds of all (281 events) summer pre-Shamal days, (b) average wind speeds of all (281 events) summer Shamal days, (c) difference between average wind speeds during summer pre-Shamals and Shamals for all 281 events, (d–f) same as (a–c) but for winter.

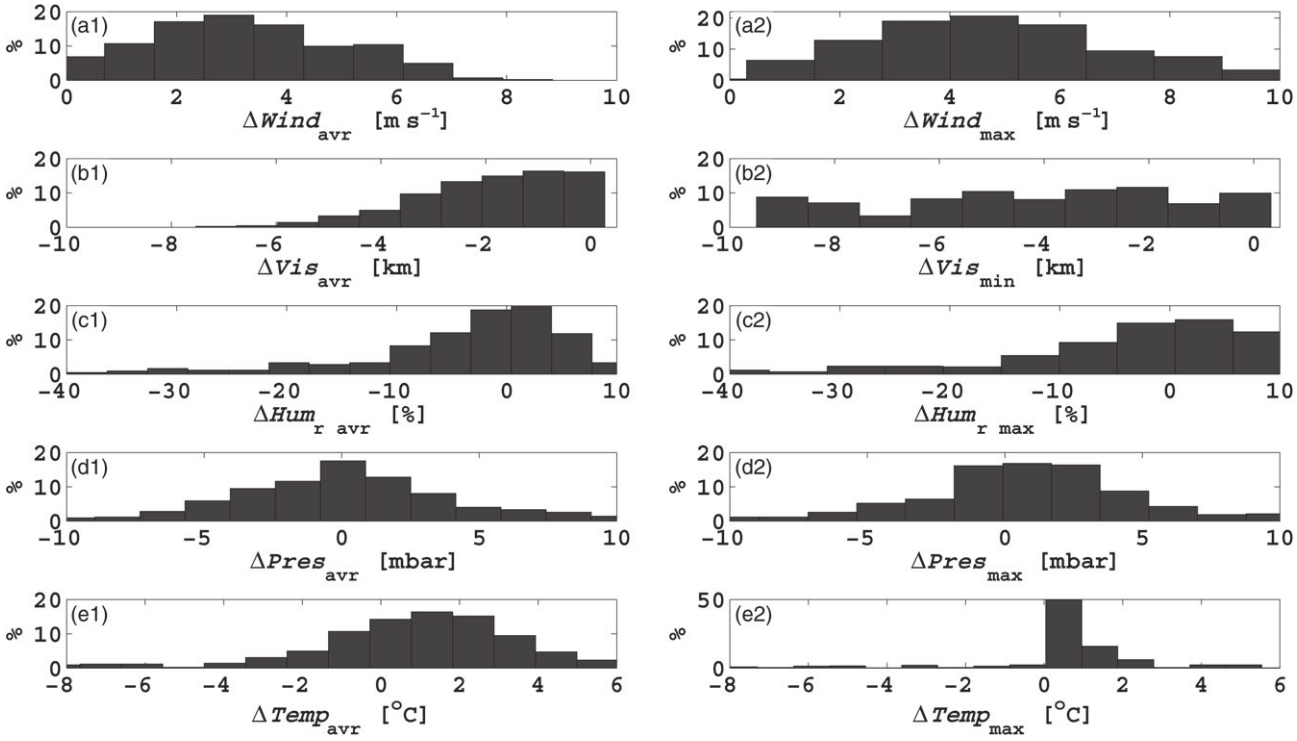

Figure 12. Histograms of differences in meteorological parameters between pre-Shamal and Shamal events (421 events, 1973–2012): (a1) average wind speed (Equation (6)), (a2) max wind speed (Equation (7)), (b1) average visibility (Equation (8)), (b2) min visibility (Equation (9)), (c1) average relative humidity (Equation (12)), (c2) max relative humidity (Equation (13)), (d1) average barometric pressure (Equation (14)), (d2) max barometric pressure (Equation (15)), (e1) average air temperature (Equation (10)), and (e2) max air temperature (Equation (11)).

Table 2. Maximum, minimum, and average differences in meteorological parameters between pre-Shamal and Shamal events (421 events, 1973–2012).

Meteorological parameter	Average	Max	Min
$\Delta Wind_{avr}$ [m s^{-1}] (Equation (6))	2.7 (0.4,5.8)	11.1	0.2
ΔVis_{avr} [km] (Equation (8))	−1.7 (−4.9,−1.1)	−7.9	−0.2
$\Delta Temp_{avr}$ [°C] (Equation (10))	0.3 (−3.9,3.5)	5.1	−7.5
$\Delta Hum_{r\,avr}$ [%] (Equation (12))	−4.3 (−25.0,6.9)	29.8	−44.5
$\Delta Pres_{avr}$ [mbar] (Equation (14))	−0.2 (−8.7,10.9)	29.5	−19.6

95% bootstrap confidence intervals are given in parentheses.

had the highest number of Shamal days (72 days), while 1992 had the lowest (4 days) (Figure 14(a)). The first quarter of the 1973–2012 period had the largest number of Shamal days (32% of the total) with the number of Shamal days declining by 46%, a change of −0.43 days year^{-1}, over the 40 year period. However, further analysis suggests that the decline in the number of Shamal days occurred mainly between 1973 and 1998 with a decrease of 0.96 days year^{-1}. Afterwards, from 1998 to 2012, the number of Shamal days per year has increased by 1.63 days year^{-1}. This increase in the number of Shamal days between 1998 and 2012 is consistent with the observed reduction in the yearly average visibility (Figure 4(f)).

There was a significant difference in the number of Shamal days as a function of the season, with 77% of Shamal days occurring in summer and only 8% in winter (Figure 14(b)); 52% of Shamal days occurred during the first part of summer (Jun–Jul), commensurate with the stationary intense summer monsoon low pressure system over NW India that affects the N Gulf (Figure 14(c)). For comparison, a study by Rao *et al.* (2001) observed an average number of 46 Shamal days year^{-1} between 1990 and 2000 in Qatar. That study suggested seasonal differences in the number of Shamal events as well, with 51% of the total Shamal days occurring during the first part of summer.

3.2.3. *Dust storms and Shamal events*

The average number of dust storms (visibility ≤1 km; (Kutiel and Furman, 2003) since 1973 is 13 storms year^{-1}, with the first half of the period (1973–1991) accounting for 76% of the dust storms (Figure 15). Furthermore, the number of dust storms has decreased by 93% since 1973. Moreover, between the years 1973 and 1998 a decrease of 0.93 dust storms year^{-1} was observed, with a more pronounced decrease of 2.04 dust storms year^{-1} from 1982 to 1998. This trend reversed between 1998 and 2010, and the number of dust storms has increased by 0.74 events year^{-1} (Figure 15). This increase is consistent with the increase in the number of dust storms observed in Riyadh, Saudi Arabia, during 2000–2010 as reported by the World Meteorological Organization (2010). Moreover, this trend

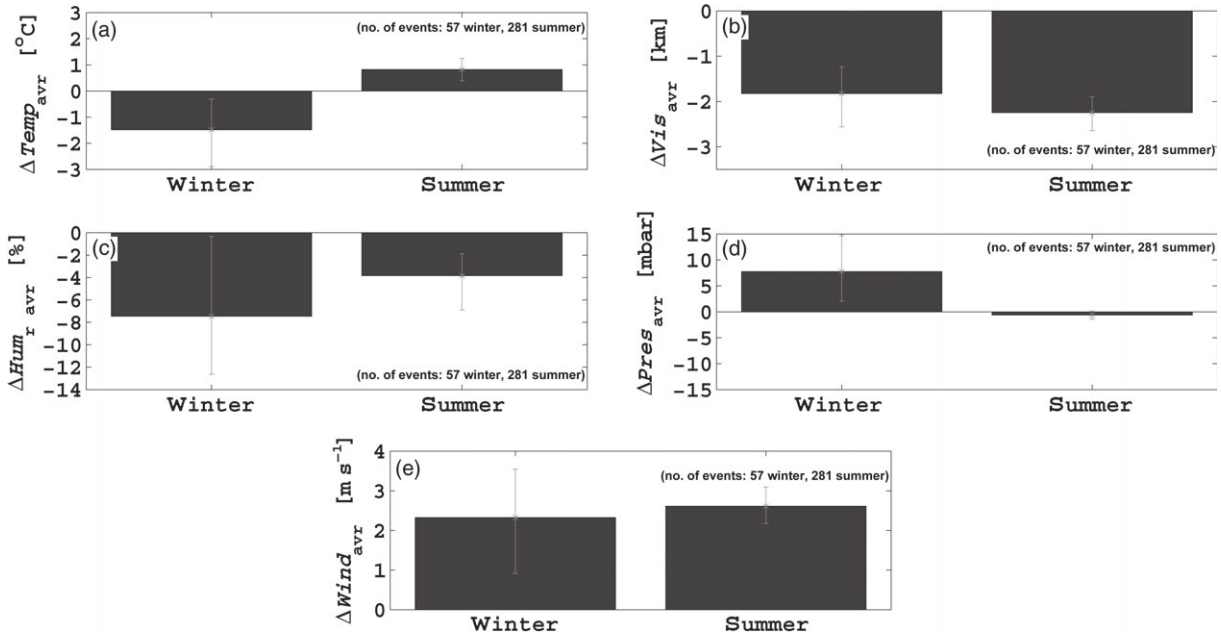

Figure 13. Average differences in meteorological parameters between pre-Shamal and Shamal events for winter (57 events) and summer (281 events): (a) air temperature (Equation (10)), (b) visibility (Equation (8)), (c) relative humidity (Equation (12)), (d) barometric pressure (Equation (14)), and (e) wind speed (Equation (6)).

Table 3. Differences in meteorological parameters between pre-Shamal and Shamal events (1973–2012) grouped into seasons.

Meteorological parameter	Average		Std deviation	
	Winter	Summer	Winter	Summer
$\Delta Wind_{avr}$ [m s^{-1}] (Equation (6))	2.3 (0.9,3.5)	2.6 (2.2,3.1)	2.3	1.8
ΔVis_{avr} [km] (Equation (8))	−1.8 (−1.2,−2.6)	−2.2 (−2.6,−1.9)	1.9	1.7
$\Delta Temp_{avr}$ [°C] (Equation (10))	−1.5 (−2.8,−0.3)	0.8 (0.4,1.2)	2.3	1.7
$\Delta Hum_{r\ avr}$ [%] (Equation (12))	−7.5 (−13.1,−0.4)	−3.8 (−7.1,−1.8)	4.4	2.5
$\Delta Pres_{avr}$ [mbar] (Equation (14))	7.8 (2.1, 14.6)	−0.6 (−1.5,−0.1)	5.5	2.7

95% bootstrap confidence intervals are given in parentheses.

is similar to that of the number of Shamal days, with a correlation of 0.42 (0.30, 0.62) between the number of Shamal days per year and number of dust storms per year (Figure 14(a)).

We note that dust storms in the region are not always associated with Shamal events. They may result also from local, short period, unstable weather systems that advect dust from the dry wash regions of Iraq or the eastern deserts of Saudi Arabia (Kutiel and Furman, 2003). Between 1973 and 2010, observations indicate that only 38% of the 495 dust storms formed during Shamal events. The observed dust storms during the study period exhibited wind speeds up to 13 m s^{-1}, caused abrupt drops in air temperature of 1.0°C (0.4, 1.7) in an hour, and reduced visibility to an average of 0.78 km (0.69, 0.85).

Similar to Shamal events, there were seasonal differences in the frequency of dust storms, with the highest number of storms observed during summer with an average of 7 storms, compared to only 1 dust storm per winter (Figure 15). The lower values during winters are a result of weaker average wind speeds (3.7 m s^{-1}) and the Mesopotamian floodplain being more resistant to wind erodibility due to relatively high (880 m^3 s^{-1}) river discharge from the Euphrates, Tigris, and other streams. In the summer, average wind speed is higher (5.3 m s^{-1}), while river streams dry out due to lower fresh water discharge (350 m^3 s^{-1}) (Iraq Foundation, 2003) resulting in a dry surface layer that is more susceptible to erosion by winds.

4. Summary and conclusions

This study focused on climate variability over a period of 40 years (1973–2012) in the N Gulf, based on observations at Kuwait, Bahrain, and NE Saudi Arabia, and the relation of Shamal events and teleconnection patterns to this variability. Results of our study indicate that over the last 40 years the climate in the region experienced a general trend of:

- Increase in temperature of 0.8°C (0.4, 1.6);
- Decrease in barometric pressure of 0.8 mbar (0.4, 1.6);
- Reduction in humidity of 5.6% (1.2, 9.6);
- Decrease in visibility of 0.8 km (0.4, 1.6).

Variability observed in air temperature, barometric pressure, and precipitation throughout the study period is suggested to be in response to the three teleconnection patterns NAO, ENSO, and IOD impacting the region. This conclusion is supported by significant ($p_{value} < 0.05$) correlations,

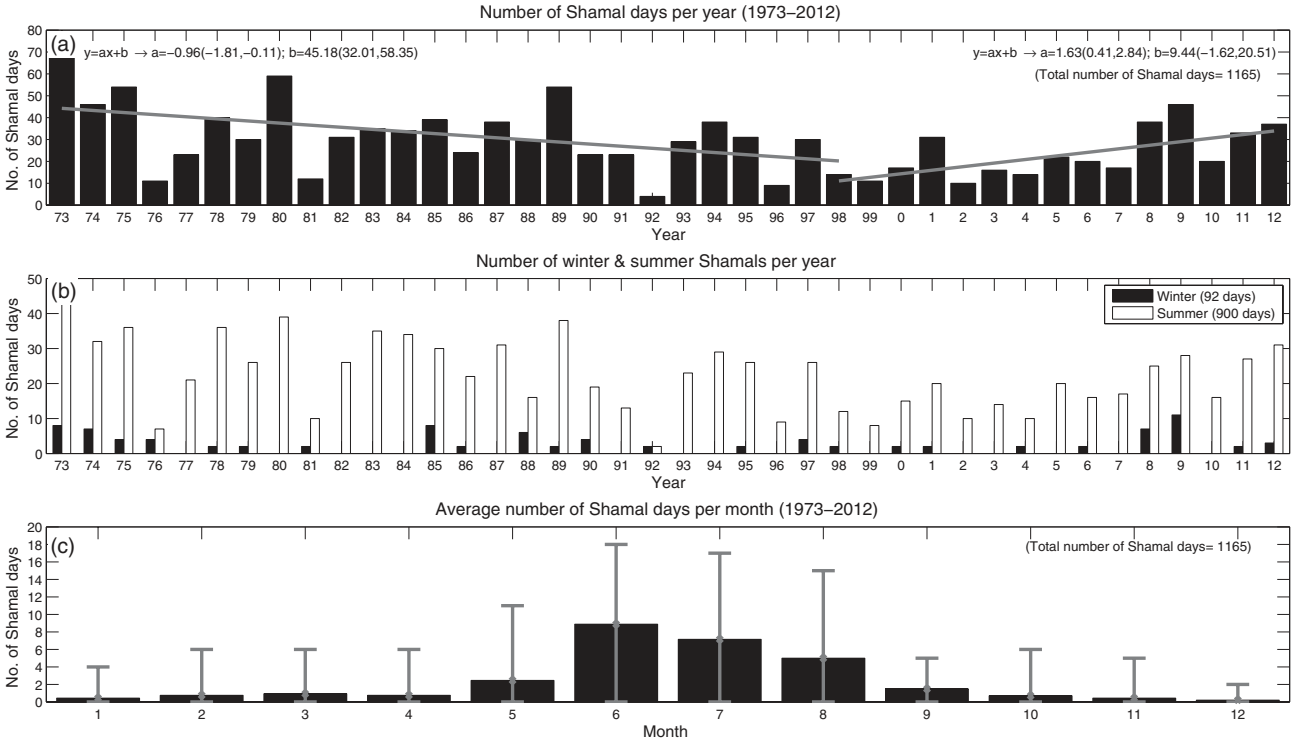

Figure 14. Number of Shamal days in 1973–2012: (a) number of Shamal days per year. A linear fit to the data, using robust regression is represented by the solid line (fit parameters are given in the top corners), (b) number of winter and summer Shamal days per year, and (c) average number of Shamal days per month with the data range indicated by whiskers.

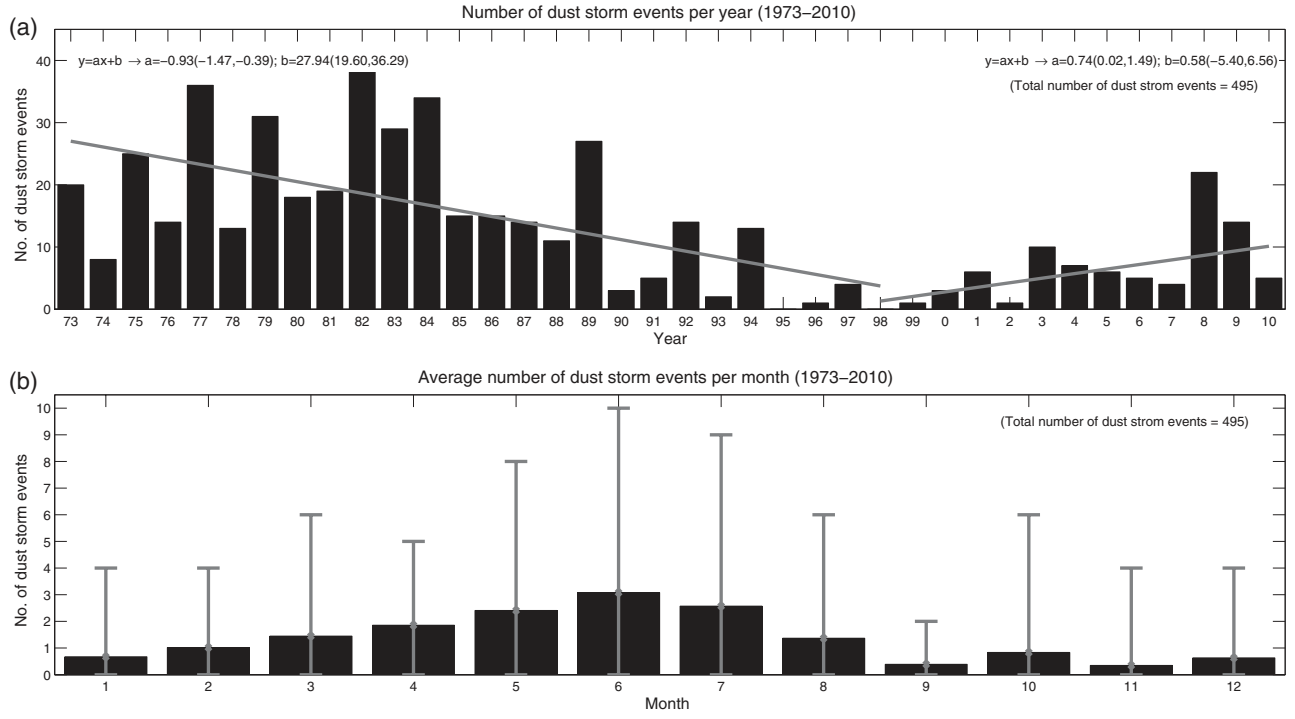

Figure 15. (a) Number of dust storms per year. A linear fit to the data, using robust regression is represented by the solid line; (b) average number of dust storms per month in 1973–2010 with their monthly maximum and minimum values indicated by whiskers.

as well as positive N_s coefficient of efficiency values between these three meteorological parameters and the teleconnection patterns indices.

Visibility variability was mainly in response to the wind speed and precipitation in the region. Furthermore, it is suggested that the result of anthropogenic activity disturbances to about a quarter of the pavement of desert areas, resulting from military activity during the 1990–1991 Gulf War and 'Operation Iraqi Freedom' in 2003, has further led to a decrease in visibility.

Relating Shamal events to climate variability necessitates an operational definition of such events, however, we could not find a standard and agreed upon definition of a Shamal in the literature. Thus, we defined a Shamal day in the present study as a WNW-N (287° < direction < 360°) wind with an hourly average speed ≥9.85 m s^{-1} blowing during at least 3 h day^{-1}. Two consecutive Shamal days are required for a Shamal to be classified as a Shamal event. On the basis of this definition, and comparison to pre-Shamal conditions, Shamal events were found to cause abrupt changes in meteorological parameters: an increase in wind speed of 2.7 m s^{-1} (0.4, 5.8), an increase in temperature during summer of 0.8°C (0.4, 1.2), and a decrease of 1.5°C (0.3, 2.8) during winter, a decrease in barometric pressure during summer of 0.6 mbar (0.1, 1.5) and a increase of 7.8 mbar (2.1, 14.6) during winter, a decrease in visibility of 1.7 km (1.1, 4.9), and reduction in humidity of 4.3% (6.9, 25.0). A total of 421 Shamal events, compromised of 1165 days, occurred during the study period, with 77% of Shamal days occurring in the summer season. The overall number of Shamal event days has decreased by 46% between 1973 and 2012. However, further analysis suggests an increase of 1.63 Shamal days year^{-1} in the last 15 years of the study period. Similarly, the number of dust storms has also increased between 1998 and 2010 at a rate of 0.74 dust storm events year^{-1}. Results of this study encourage future observational and numerical studies of the Gulf's response (physically and biologically) to local weather events, e.g. dust storms, as well as teleconnection patterns.

Furthermore, the significance of Shamal events through their effect on the momentum and heat exchanges at the air–sea interface has motivated a detailed observational meteorological (surface shortwave/longwave radiation, air temperature, SST, humidity, barometric pressure, and wind speed/direction) and oceanographic (currents, temperature, salinity, and dissolved oxygen structures) study in the N Gulf. This study, which is currently in progress, is focusing on the winter, and fall, and spring transition periods.

Acknowledgements

We thank Mr. Hassan Dashti, Mr. Mohamed Karam, and Mr. Nawaf Hassan of the Kuwait Meteorological Office for providing the observational data. We also thank NCEP and ECMWF-IFS for providing online access to reanalysis data. We are also grateful to NOAA-NCDC, NOAA-CPC, and JAMSTEC for the online teleconnection pattern data. This study was partly funded by the Kuwait Foundation for the Advancement of Sciences, project number 2012-6401-03. We are further grateful to the three anonymous referees for their constructive comments.

Appendix

Dust aerosol optical properties at 550 nm wavelength (Benedetti *et al.*, 2009).

Dust type	α_{ei} [m^2 g^{-1}]	ω	g
0.03–0.55 μm	2.6321	0.9896	0.7300
0.66–0.90 μm	0.8679	0.9672	0.5912
0.90–20.0 μm	0.4274	0.9441	0.7788

References

Al-dousari ALIM, Al-awadhi J. 2012. Dust fallout in northern Kuwait, major sources and characteristics. *Kuwait J. Sci.* **39**: 171–187.

Ali A. 1994. *Wind Meteorology of the Summer Shamal in the Arabian Gulf Region*. Master's thesis, Boston University, Boston, MA.

Almazroui M, Islam MN, Jones P, Athar H, Rahman MA. 2012a. Recent climate change in the Arabian Peninsula: seasonal rainfall and temperature climatology of Saudi Arabia for 1979–2009. *Atmos. Res.* **111**: 29–45.

Almazroui M, Nazrul Islam M, Athar H, Jones PD, Rahman MA. 2012b. Recent climate change in the Arabian Peninsula: annual rainfall and temperature analysis of Saudi Arabia for 1978–2009. *Int. J. Climatol.* **32**(6): 953–966.

Arpe K, Leroy SAG. 2009. Atlantic hurricanes testing impacts of local SSTs, ENSO, stratospheric QBO implications for global warming. *Quat. Int.* **195**(12): 4–14.

Arun C, Swadhin B, Mujumdar M, Ohba R, Yamagata T. 2005. Diagnosis of tropospheric moisture over Saudi Arabia and influences of IOD and ENSO. *Mon. Weather Rev.* **134**: 598–617.

Attrill MJ. 2009. Sea temperature change as an indicator of global change. In *Climate Change*, Letcher TM (ed). Elsevier: Amsterdam, 337–347.

Barlow M, Wheeler M, Lyon B, Cullen H. 2005. Modulation of daily precipitation over Southwest Asia by the Madden Julian Oscillation. *Mon. Weather Rev.* **133**(12): 3579–3594.

Barnston A, Livezey R. 1987. Classification, seasonality and persistence of low-frequency atmospheric circulation patterns. *Mon. Weather Rev.* **115**(6): 1083–1126.

Bartlett KS. 2004. *Dust Storm Forecasting For Al Udeid Ab, Qatar: An Empirical Analysis*. Master's thesis, Air University, Islamabad.

Benedetti A, Morcrette J-J, Boucher O, Dethof A, Engelen RJ, Fisher M, Flentje H, Huneeus N, Jones L, Kaiser JW, Kinne S, Mangold A, Razinger M, Simmons AJ, Suttie M. 2009. Aerosol analysis and forecast in the European Centre for Medium-Range Weather Forecasts Integrated Forecast System: 2. Data assimilation. *J. Geophys. Res.* **114**: 1–18.

Blasing T. 2013. *Recent greenhouse gas concentrations*. http://cdiac.ornl.gov/pns/current_ghg.html (accessed 3 March 2013).

Chang C, Harr P, Ju J. 2000. Possible roles of Atlantic circulations on the weakening Indian monsoon rainfall ENSO relationship. *J. Clim.* **14**: 2376–2380.

Chao S-Y, Kao TW, Al-Hajri KR. 1992. A numerical investigation of circulation in the Arabian Gulf. *J. Geophys. Res.* **97**(C7): 11219–11236.

Chin M et al. 2002. Tropospheric aerosol optical thickness from the GOCART model and comparisons with satellite and sun photometer measurements. *J. Atmos. Sci.* **59**: 461–483.

Clements T, Stone R, Mann J, Eymann J. 1963. A study of windborne sand and dust in desert areas. Technical report No. ES-8, University of South California, Los Angeles, CA.

Cohen J, Barlow M. 2005. The NAO, the AO, and global warming: how closely related? *J. Clim.* **18**(21): 4498–4513.

Crook J. 2009. *Climate Analysis and Long Range Forecasting of Dust Stroms in Iraq*. Master's thesis, Naval Postgraduate School, Monterey, CA.

Cullen H, Demenocal P. 2000. North Atlantic influence on Tigris Euphrates. *Int. J. Climatol.* **863**: 853–863.

Dai A. 2006. Recent climatology, variability, and trends in global surface humidity. *J. Clim.* **19**(15): 3589–3606.

Donat MG, Peterson TC, Brunet M, King AD, Almazroui M, Kolli RK, Djamel Boucherf, Anwar Yousuf Al-Mulla, Abdourahman Youssouf Nour, Ahmed Attia Aly, Tamer Ali Ali Nada, Muhammad M Semawi, Hasan Abdullah Al Dashti, Tarek G Salhab, Khalid I El Fadli, Mohamed K Muftah, Sidaty Dah Eida, Wafae Badi, Fatima Driouech, Khalid El Rhaz, Mohammed JY Abubaker, Ayman S Ghulam, Amani Sanhouri Erayah, Maher Ben Mansour, Waleed O Alabdouli, Jemie Salem Al Dhanhani, Majed N Al Shekaili. 2014. Changes in extreme temperature and precipitation in the Arab region: long-term trends and variability related to ENSO and NAO. *Int. J. Climatol.* **34**(3): 581–592.

Eager RE, Raman S, Wootten A, Westphal DL, Reid JS, Al Mandoos A. 2008. A climatological study of the sea and land breezes in the Arabian Gulf region. *J. Geophys. Res.* **113**(D15): D15106.

Efron B, Tibshirani R. 1986. Bootstrap methods for standard errors, confidence intervals, and other measures of statistical accuracy. *Stat. Sci.* **1**(1): 54–75.

El Kenawy A, López-Moreno JI, Vicente-Serrano SM. 2012. Trend and variability of surface air temperature in northeastern Spain (1920–2006): linkage to atmospheric circulation. *Atmos. Res.* **106**: 159–180.

Elsanabary MH, Gan TY. 2013. Wavelet analysis of seasonal rainfall variability of the Upper Blue Nile Basin, its teleconnection to global sea surface temperature, and its forecasting by an artificial neural network. *Mon. Weather Rev.* **142**(5): 1771.

EPA. 2012. *Climate change*. http://www.epa.gov/climatechange/ (accessed 3 March 2013).

Giannakopoulou EM, Toumi R. 2012. The Persian Gulf summertime low-level jet over sloping terrain. *Q. J. R. Meteorol. Soc.* **138**(662): 145–157.

Goes JI, Thoppil PG, Gomes HDR, Fasullo JT. 2005. Warming of the Eurasian landmass is making the Arabian Sea more productive. *Science* **308**(5721): 545–547.

Goudie AS. 2009. Dust storms: recent developments. *J. Environ. Manag.* **90**(1): 89–94.

Gupta HV, Kling H. 2011. On typical range, sensitivity, and normalization of Mean Squared Error and Nash-Sutcliffe Efficiency type metrics. *Water Resour. Res.* **47**(W10601): 1–3.

Hansen J, Lacis A, Rind D, Russell G, Stone P, Fung I, Ruedy R, Lerner J. 1984. Climate sensitivity: analysis of feedback mechanisms. In *Climate Processes and Climate Sensitivity*, Vol. 5, Hansen JE, Takahashi T (eds). American Geophysical Union: Washington DC, 130–163.

Hollingsworth A, Engelen RJ, Benedetti A, Dethof A, Flemming J, Kaiser JW, Morcrette J-J, Simmons AJ, Textor C, Boucher O, Chevallier F, Rayner P, Elbern H, Eskes H, Granier C, Peuch V-H, Rouil L, Schultz MG. 2008. Toward a monitoring and forecasting system for atmospheric composition: the GEMS project. *Bull. Am. Meteorol. Soc.* **89**(8): 1147–1164.

Huber PJ, Ronchetti EM. 2009. Generalities. In *Robust Statistics*, 2nd edn. John Wiley & Sons: New York, NY.

Hurrell J. 1995. Decadal trends in the North Atlantic Oscillation: regional temperatures and precipitation. *Science* **269**(5224): 676–679.

IPCC. 2014. Climate change 2014: impacts, adaptation, and vulnerability. Part A: global and sectoral aspects. Contribution of Working Group II to the Fifth Assessment Report of the Intergovernmental Panel on Climate Change. Technical report, October 2013, UNEP, New York, NY.

Iraq Foundation. 2003. Physical characteristics: Mesopotamian marshlands of southern Iraq. http://www.iraqfoundation.org/edenagain/publications/pdfs/physicalcharreport.pdf (accessed 3 March 2013).

Janabi H. 2010. Water security in Iraq. Technical report, UN Food and Agriculture Organization, Rome.

Jin F-F. 2003. Strong El Niño events and nonlinear dynamical heating. *Geophys. Res. Lett.* **30**(3): 1120.

Jones PD. 2003. Global change: surface temperature trends. In *Encyclopedia of Atmospheric Sciences*, Holton JR (ed). Academic Press: Oxford, UK, 898–910.

Jones P, Wigley T, Wright P. 1986. Global temperature variations between 1861 and 1984. *Nature* **322**: 430–434.

Joseph P, Eischeid J, Pyle R. 1994. Interannual variability of the onset of the Indian summer monsoon and its association with atmospheric features, El Niño, and sea surface temperature anomalies. *J. Clim.* **7**(81): 81–105.

Kanamitsu M, Ebisuzaki W, Woollen J, Yang S-K, Hnilo JJ, Fiorino M, Potter GL. 2002. NCEPDOE AMIP-II reanalysis (R-2). *Bull. Am. Meteorol. Soc.* **83**(11): 1631–1643.

Koch M, El-Baz F. 1998. Identifying the effects of the Gulf War on the geomorphic features of Kuwait by remote sensing and GIS. *Photogramm. Eng. Remote Sens.* **64**(7): 739–747.

Kumar KN, Ouarda TBMJ. 2014. Precipitation variability over UAE and global SST teleconnections. *J. Geophys. Res. Atmos.* **119**: 1–10.

Kutiel H, Furman H. 2003. Dust storms in the Middle East: sources of origin and their temporal characteristics. *Indoor Built Environ.* **12**(6): 419–426.

Leroy SA. 2006. From natural hazard to environmental catastrophe: past and present. *Quat. Int.* **158**(1): 4–12.

Meehl G, Loon HV. 1979. The seesaw in winter temperatures between Greenland and Northern Europe. Part III: teleconnections with lower latitudes. *Mon. Weather Rev.* **107**(9): 1095–1106.

Mirza MMQ. 2002. Global warming and changes in the probability of occurrence of floods in Bangladesh and implications. *Glob. Environ. Change* **12**(2): 127–138.

Morcrette J-J, Beljaars A, Benedetti A, Jones L, Boucher O. 2008. Sea-salt and dust aerosols in the ECMWF IFS model. *Geophys. Res. Lett.* **35**(24): 1–5.

Naidu C, Satyanarayana G, Durgalakshmi K, Malleswara Rao L, Jeevana Mounika G, Raju AD. 2012. Changes in the frequencies of northeast monsoon rainy days in the global warming. *Glob. Planet. Change* **92–93**: 40–47.

NASA. 2013. *Earth science data and information system*. https://lance-modis.eosdis.nasa.gov/imagery/subsets/?area=af (accessed 3 March 2013).

Nash J, Sutcliffe J. 1970. River flow forecasting through conceptual models part I: a discussion of principles. *J. Hydrol.* **10**(3): 282–290.

Nasrallah H, Balling R. 1995. Impact of desertification on temperature trends in the Middle East. *Environ. Monit. Assess.* **37**(1-3): 265–271.

Nasrallah HA, Nieplova E, Ramadan E. 2004. Warm season extreme temperature events in Kuwait. *J. Arid Environ.* **56**(2): 357–371.

Partow H. 2001. The Mesopotamian Marshlands: demise of an ecosystem. Technical report, United Nations Environment Programme.

Perrone T. 1979. Winter Shamal in the Persian Gulf, Technical Report 79-06. Technical report, Naval Environmental Prediction Research Facility, Monterey, CA.

Philandras C, Nastos P, Kapsomenakis I, Repapis C. 2013. Climatology of upper air temperature in the Eastern Mediterranean region. *Atmos. Res.* **152**: 29–42.

Preining O. 1992. Global warming: greenhouse gases versus aerosols. *Sci. Total Environ.* **126**(12): 199–204.

Press W, Teukolsky S, Vetterling W, Flannery B. 2007. *Numerical Recipes: The Art of Scientific Computing*, 3rd edn. Cambridge University Press: Cambridge, UK.

Privett D. 1959. Monthly charts of evaporation from the N. Indian Ocean (including the Red Sea and the Persian Gulf). *Q. J. R. Meteorol. Soc.* **85**(366): 424–428.

Rao PG, Al-Sulaiti M, Al-Mulla AH. 2001. Winter Shamals in Qatar, Arabian Gulf. *Weather* **56**(12): 444–451.

Rao PG, Al-Sulaiti MH, Al-Mulla AH. 2003. Summer Shamals over the Arabian Gulf. *Weather* **58**: 471–478.

Reddy MS. 2005. Estimates of global multicomponent aerosol optical depth and direct radiative perturbation in the Laboratoire de Météorologie Dynamique general circulation model. *J. Geophys. Res.* **110**: D10S16.

Reynolds RM. 1993. Physical oceanography of the Persian Gulf, Strait of Hormuz, and the Gulf of Oman: results from the Mt. Mitchell expedition. *Mar. Pollut. Bull.* **27**: 35–59.

Saeed TM, Al-Dashti H, Spyrou C. 2014. Aerosol's optical and physical characteristics and direct radiative forcing during a Shamal dust storm, a case study. *Atmos. Chem. Phys.* **14**(7): 3751–3769.

Saji NH, Yamagata T. 2003. Possible impacts of Indian Ocean Dipole mode events on global climate. *Clim. Res.* **25**: 151–169.

Saji NH, Goswami BN, Vinayachandran PN, Yamagata T. 1999. A dipole mode in the tropical Indian Ocean. *Nature* **401**(6751): 360–363.

Shakula J, Paolino D. 1983. The southern oscillation and long-range forecasting of the summer monsoon rainfall over India. *Mon. Weather Rev.* **111**: 1830–1837.

Soman K, Slingo J. 1997. Sensitivity of the Asian summer monsoon to aspects of sea-surface-temperature anomalies in the tropical Pacific Ocean. *Q. J. R. Meteorol. Soc.* **123**: 309–336.

Thoppil PG, Hogan PJ. 2010. Persian Gulf response to a wintertime Shamal wind event. *Deep-Sea Res. I Oceanogr. Res. Pap.* **57**(8): 946–955.

Torrence C, Webster P. 1999. Interdecadal changes in the ENSO monsoon system. *J. Clim.* **12**: 2679–2690.

UCAR/COMET. 2010. *Forecasting Dust Storms v2*. http://www.meted.ucar.edu/mesoprim/dust/ (accessed 3 March 2013).
UNEP. 2013. *Forecasting and early warning of dust storms*. http://www.unep.org/geas/ (accessed 3 March 2013).
Vishkaee F, Flamant C, Cuesta J, Oolman L, Flamant P, Khalesifard HR. 2012. Dust transport over Iraq and northwest Iran associated with winter Shamal: a case study. *J. Geophys. Res.* **117**(D3): D03201.
van Vliet MT, Franssen WH, Yearsley JR, Ludwig F, Haddeland I, Lettenmaier DP, Kabat P. 2013. Global river discharge and water temperature under climate change. *Glob. Environ. Change* **23**: 450–464.
Walker G, Bliss E. 1937. World weather, VI. *Mem. R. Meteorol. Soc.* **39**: 119–139.
Walters K. 1990. The Persian Gulf Region, a climatological study. Technical report, United States Air Force, Asheville, NC.
Webster P. 1995. The annual cycle and the predictability of the tropical coupled ocean-atmosphere system. *Meteorog. Atmos. Phys.* **56**: 33–55.
Webster PJ, Magafia VO, Palmer TN, Shukla J, Tomas RA, Yanai M, Yasunari T. 1998. Monsoons: processes, predictability, and the prospects for prediction. *J. Geophys. Res.* **103**: 14451–14510.
Webster PJ, Moore AM, Loschnigg JP, Leben RR, Nin E. 1999. Coupled ocean-atmosphere dynamics in the Indian Ocean during 1997–98. *Nature* **401**(6751): 356–360.
Wilkerson W. 1991. Dust and sand forecasting in Iraq and adjoining countries. Technical report, Air Weather Service, Scott Air Force Base, IL.
WMO. 2010. A decade of climate extremes 2001–2010 (WMO-No. 1103). Technical Report 1103, World Meteorological Organization, Geneva, Switzerland.
Yosef Y, Saaroni H, Alpert P. 2009. Trends in daily rainfall intensity over Israel 1950/1–2003/4. *Open Atmos. Sci. J.* **3**(1): 196–203.
Zhao Q, He K, Rahn KA, Ma Y, Jia Y, Yang F, Duan F, Lei Y, Chen G, Cheng Y, Liu H, Wang S. 2010. Dust storms come to Central and Southwestern China, too: implications from a major dust event in Chongqing. *Atmos. Chem. Phys.* **10**(6): 2615–2630.